Salt-Mediated Oligomerization of the Mouse Prion Protein Monitored by Real-Time NMR

Ishita Sengupta, Suhas H. Bhate, Ranabir Das and Jayant B. Udgaonkar

National Centre for Biological Sciences, *Tata Institute of Fundamental Research, Bengaluru 560065, India*

Correspondence to Ranabir Das and Jayant B. Udgaonkar:. *rana@ncbs.res.in; jayant@ncbs.res.in*
http://dx.doi.org/10.1016/j.jmb.2017.05.006
Edited by Sheena Radford

Abstract

The prion protein forms β-rich soluble oligomers *in vitro* at pH 4 in the presence of physiological concentrations of salt. In the absence of salt, oligomerization and misfolding do not take place in an experimentally tractable timescale. While it is well established that a lowering of pH facilitates misfolding and oligomerization of this protein, the role of salt remains poorly understood. Here, solution-state NMR was used to probe perturbations in the monomeric mouse prion protein structure immediately upon salt addition, prior to the commencement of the oligomerization reaction. The weak binding of salt at multiple sites dispersed all over the monomeric protein causes a weak and non-specific perturbation of structure throughout the protein. The only significant perturbation occurs in the loop between helix 2 and 3 in and around the partially buried K193–E195 salt bridge. The disruption of this key electrostatic interaction is the earliest detectable change in the monomer before any major conformational change occurs and appears to constitute the trigger for the commencement of misfolding and oligomerization. Subsequently, the kinetics of monomer loss, due to oligomerization, was monitored at the individual residue level. The oligomerization reaction was found to be rate-limited by association and not conformational change, with an average reaction order of 2.6 across residues. Not surprisingly, salt accelerated the oligomerization kinetics, in a non-specific manner, by electrostatic screening of the highly charged monomers at acidic pH. Together, these results allowed a demarcation of the specific and non-specific effects of salt on prion protein misfolding and oligomerization.

Introduction

The ultimate proof of the protein-only hypothesis [1,2] of prion propagation lies in the *in vitro* generation of infectious prion particles [3]. To this end, several laboratories have developed protocols for synthetic prion preparations [4], failing, however, to replicate infectivity titers typically reported for diseased individuals despite maintaining significant toxicity [5–7]. Despite this shortcoming, two key results have emerged from these efforts: (i) oligomers can be as toxic as amyloid fibrils [8,9] and (ii) the clinical symptoms of disease need not be correlated with amyloid deposition [10,11]. Indeed, oligomers composed of 14–28 monomers have been found to constitute the most infectious prion particles [12].

Not surprisingly then, recent focus has shifted to establishing the molecular mechanism of oligomer formation [13–16], with much emphasis on the identification of aggregation-prone monomeric intermediates [17–23], which lead directly to the formation of these oligomers. *In vitro*, solution conditions have been found to dictate the aggregated form of the prion protein: β-rich soluble oligomers are formed at acidic pH, whereas amyloid fibrils are formed at neutral pH [24].

The misfolding and oligomerization of WT mouse prion protein (moPrP) occur readily at acidic pH, with the transition midpoint at pH 4.7 [25]. Either H186 (mouse numbering has been used throughout the manuscript) or D201 has to be protonated for oligomerization to occur [26]. At neutral pH, oligomerization cannot be observed because only a very small fraction of moPrP molecules have either H186 or D201 protonated. The soluble oligomers that form at pH 4 and in 150 mM NaCl have been shown to be β-sheet-rich, with a hydrodynamic radius of ~16 nm

[25]. The major conformational changes that take place during oligomerization are confined to the C-terminal domain (CTD) [27]. However, the middle hydrophobic region in the N-terminal region (NTR) plays an important role in the association of monomers [28]. It should also be mentioned that *in vivo*, the prion protein encounters acidic pH during its trafficking through the endocytic pathway, where it may undergo conversion into its pathogenic counterpart [29–31].

Remarkably, susceptibility to prion disease is dictated by the propensity to form β-sheet-rich oligomers [32], among other factors, and *in vitro*, generated oligomers have been shown to disrupt membranes pointing toward a potential mechanism for their toxicity [33,25]. Importantly, regardless of the solution conditions, oligomer preparations are always β-sheet-rich and, in some cases, cytotoxic [34,35], establishing them as excellent mimics of the misfolded and aggregated variant of the prion protein. More importantly, structural studies on the oligomers of the prion protein generated *in vitro* have established that their core is mostly confined to the CTD of the protein [36,33,15,28], similar but not identical to what has been observed for brain-derived prion aggregates [37].

To identify key interactions, the disruption of which may trigger misfolding, the effect of environmental conditions [38,24,39–42] and pathogenic mutations [43–51,27] on monomer structure have been investigated in much detail by both simulations and experiments. In particular, pathogenic mutations D177N, H186R, E195K, D201N, and R207H (mouse numbering) are believed to disrupt key salt bridges and destabilize the monomeric protein and accelerate misfolding and oligomerization. Interestingly, these pathogenic mutations were found to result in increased structural dynamics in alpha helix 1 (α1), the loop between α1 and beta-strand 2 (β2), and the loop between alpha helix 2 (α2) and 3 (α3) [26] in the monomer. These and other results together suggest that the initiating event in prion protein oligomerization is the separation of subdomains of the globular CTD of the protein [40,36,52,53,15,54]. Notably, the presence of salt is essential for misfolding and oligomerization to proceed in an experimentally tractable timescale, even under misfolding-promoting acidic conditions [23]. The role of salt is, however, not well understood.

In this study, real-time solution NMR spectroscopy was used to probe perturbations in the monomeric protein, which occur immediately upon the addition of NaCl at acidic pH prior to oligomerization. Subtle structural perturbations are unlikely to be observed when probing the oligomerization kinetics with circular dichroism (CD) and hydrogen-exchange (HX), as these probes rely on large changes in conformation or protection to solvent, respectively. Moreover, these kinetic experiments carried out in the presence of salt directly probe residue-specific perturbations in the monomeric protein that might trigger misfolding and oligomerization. Many of these perturbations are likely to escape detection in equilibrium experiments carried out in the absence of salt. Subsequently, oligomerization-induced signal loss from residues in the monomeric protein was monitored by NMR in a real-time manner.

The results suggest that salt plays a dual role in facilitating both misfolding and oligomerization. While the disruption of a key salt-bridge between residues K193 and E195 appears to be the earliest detectable perturbation in the monomeric protein that triggers misfolding and oligomerization, a non-specific charge-screening effect facilitates protein–protein association leading to oligomer formation. The core of the oligomers is mostly confined to the CTD, whereas the unstructured NTR and a small subset of CTD residues remain dynamic in the oligomer. Oligomerization takes place in multiple steps by the addition of monomers and is rate-limited by association. New resonances from dynamic regions of the growing oligomeric species serve as additional probes of oligomerization kinetics.

Results

The prion protein forms misfolded oligomers *in vitro* under acidic conditions (pH 4) upon the addition of physiological concentrations (150 mM) of NaCl [55,56,41,25]. The oligomerization reaction is accompanied by drastic conformational changes from an α-helical monomeric conformation to a β-sheet rich multimeric form (Fig. S1).

CSPs in the monomeric prion protein induced by the apparent binding of NaCl

The backbone ^{15}N, ^{13}C, ^{1}H chemical shifts and the $^{13}C^{\beta}$ chemical shifts were assigned for moPrP at pH 4 by standard triple resonance experiments (details in Materials and Methods). To study the interactions between moPrP and NaCl, ^{15}N, ^{1}H-edited heteronuclear single quantum coherence (HSQC) spectra were acquired at different NaCl concentrations ranging from 0 to 200 mM.

The addition of NaCl to the monomeric full-length moPrP at pH 4 to initiate misfolding and oligomerization did not perturb the overall fold of the monomeric protein, as determined by CD measurements (Fig. S2). Chemical shift changes were, however, observed in the NMR spectrum. With an increase in concentration of NaCl, a small subset of amide peaks were observed to gradually shift, as can be seen for representative residues H60, E195, Q211, and T191 in Fig. 1A. As demonstrated in Fig. 1B, residues H60, T191, E195, Q211, and K219 displayed significant perturbations upon the addition of NaCl, while residues G65, G123, and W31 were

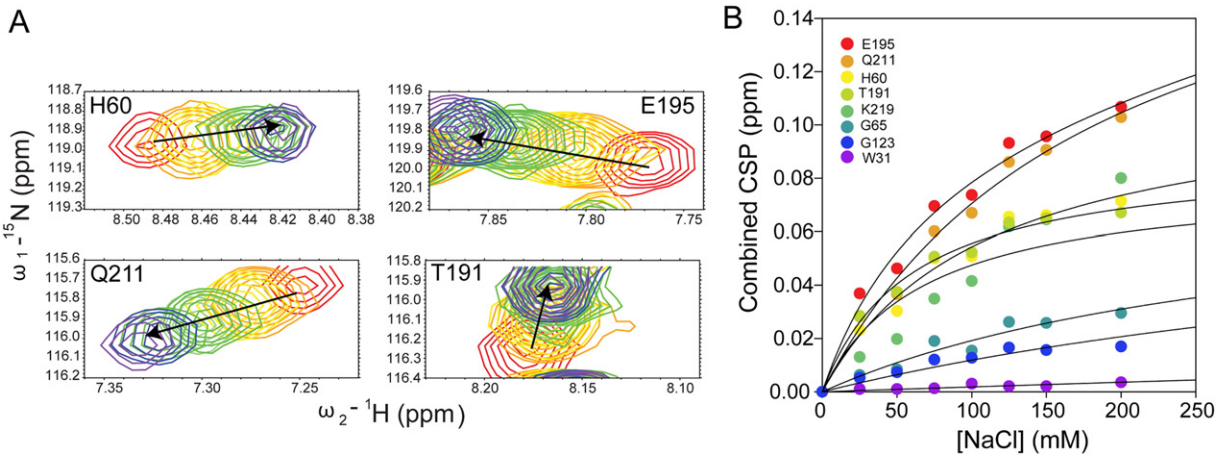

Fig. 1. Binding of NaCl to moPrP. (A) NaCl titration of ^{15}N-labeled moPrP in 10 mM sodium acetate (pH 4.0), as monitored by 2D ^{15}N–^{1}H HSQC spectra. The concentrations of NaCl used were 0 (red), 25 (orange), 50 (yellow), 75 (yellow-green), 100 (green), 125 (dark-cyan), 150 (blue), and 200 (purple) mM. The protein concentration was kept fixed at 100 μM. A separate sample was used for each NaCl concentration. Representative residues H60, E195, Q211, and T191 showing highest CSPs upon binding to NaCl can be seen to move with increasing NaCl concentration. Arrows indicate the direction of peak movement. (B) Combined amide CSPs for eight representative residues upon titration of NaCl. Residues G65, G123, and W31 show negligible CSPs upon NaCl titration, whereas residues K219, T191, H60, Q211, and E195 show large CSPs. Lines have been drawn by inspection only.

unperturbed. The dependence of the observed chemical shift perturbations (CSPs) on NaCl concentration is reminiscent of a binding curve that describes the weak binding of NaCl to monomeric moPrP.

These salt-induced CSPs were accompanied by a ~50% loss in signal [Fig. S3 and Eq. (1)] but negligible changes in line width (see later). Importantly, these CSPs remained unaltered throughout the course of the oligomerization reaction (see later). The combined amide CSPs [Eq. (2)] ranged from 0.002 ppm to 0.12 ppm across all assigned residues at 150 mM NaCl concentration (Fig. 2B). The residues with the highest CSPs (i.e., greater than mean + 3 s.d.) in the CTD were K193, E195, and Q211. When mapped onto the structure of moPrP (Fig. 2C), a major localized perturbation was observed only in the loop between α2 and α3, including a salt bridge between residues K193 and E195 and residues T191 and G194 in its vicinity. This indicated that the perturbation of this salt bridge could be a key event in triggering the misfolding and oligomerization of the prion protein.

Oligomerization of E195K moPrP at pH 5.5

The misfolding and oligomerization of WT moPrP require that H186, whose pKa is 4.7, be protonated. Hence, very little oligomerization of WT moPrP can be detected at pH 5.5 in the presence of salt. To further probe the effect of the disruption of the K193–E195 salt bridge on the misfolding and oligomerization of moPrP, the pathogenic mutant variant E195K moPrP was oligomerized at pH 4 and 5.5 in the presence of 150 mM NaCl. While both E195K and WT moPrP had completely oligomerized into a β-sheet-rich oligomer in 24 h at pH 4, only E195K moPrP showed substantial misfolding at pH 5.5 in the presence of 150 mM NaCl (Fig. 3). WT moPrP remained α-helical after 24 h at pH 5.5 (Fig. 3) and showed negligible signal change in intensity in NMR experiments (Fig. S4). The E195K moPrP protein precipitated at pH 6 and above.

Oligomerization of WT moPrP at pH 4 in the presence of different salts

To test if the oligomerization of WT moPrP at pH 4 was anion-dependent, different concentrations of Na_2SO_4 and NaBr were also used to induce oligomerization. At 24 h, the extent of oligomerization induced by 20 mM Na_2SO_4 was the same as that induced by 150 mM NaCl, while 150 mM NaBr did not induce any oligomerization. Interestingly, $MgCl_2$ was also able to induce oligomerization of the protein at chloride concentrations comparable to NaCl (Fig. 4). The Debye–Hückel screening distances for 20 mM Na_2SO_4 (ionic strength = 0.06 M) and 150 mM NaCl (ionic strength = 0.15 M) are 12.6 and 7.9 Å, respectively. The distance separating the K193 and E195 side chains is 3.4 Å; hence, in 20 mM Na_2SO_4 or in 150 mM NaCl, damping of the electrostatic interactions in the K193–E195 salt bridge by Debye–Hückel screening would occur only to the extent of about 30%. Thus, the perturbation of the K193–E195 salt bridge observed in the presence of 150 mM NaCl (Figs. 1 and 2) could not have been affected only by

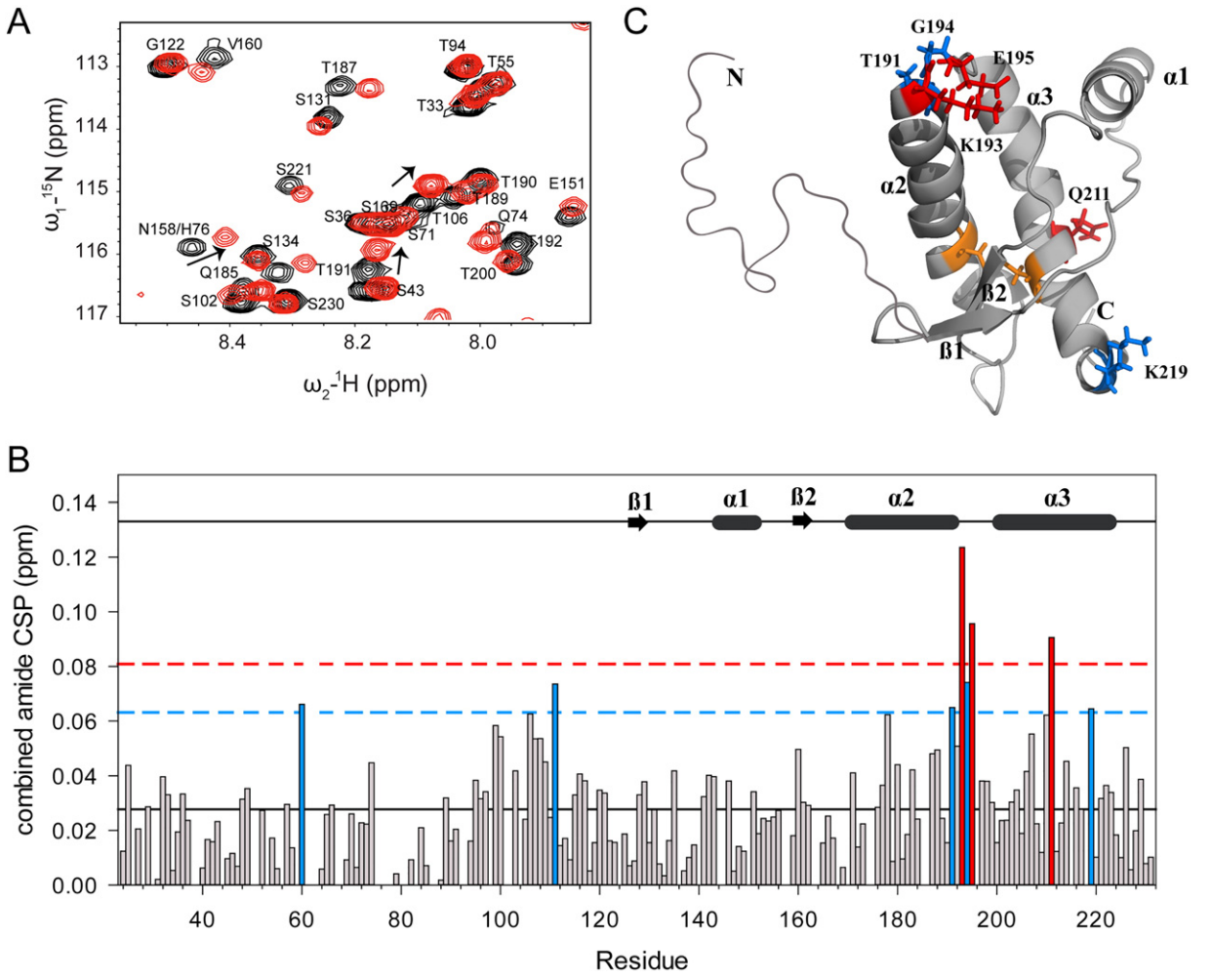

Fig. 2. Chemical shift perturbations in the 2D ^{15}N–^{1}H HSQC spectrum of 100 μM moPrP upon the initiation of aggregation with 150 mM NaCl at pH 4 and 37 °C. (A) Small section of the ^{15}N–^{1}H HSQC spectrum for 100 μM moPrP in native buffer, 10 mM sodium acetate, (pH 4.0; black), and in aggregation buffer, 10 mM sodium acetate, 150 mM NaCl (pH 4.0; red) after 1 h into the oligomerization reaction at 37 °C. The acquisition time for each spectrum was ~1 h. Cross-peaks corresponding to residues N158/H76, T106, and T191 can be seen to shift significantly upon the addition of salt (marked by arrows). The line widths remain unchanged (data not shown). (B) Combined amide CSPs [Eq. (2)] for all assigned residues of moPrP upon the initiation of oligomerization with 150 mM NaCl. The mean, mean + 2 s.d., and mean + 3 s.d. are shown by solid black, dashed blue, and dashed red lines, respectively. Residues displaying highest CSPs (> mean + 2 and 3 s.d.) have been colored blue and red. Unassigned residues have been left blank. (C) Residues showing the highest CSPs (> mean + 2 or 3 s.d) from Fig. 1B (indicated by blue and red sticks, respectively) mapped onto the structure of the CTD of moPrP (PDB entry 1AG2) [57]. The disulfide bond is shown with orange sticks. The N and C termini and the secondary structure elements have been indicated.

mobile ions but would have also involved specific binding of the anion to the protein in the vicinity of the salt bridge.

Monomer-loss kinetics monitored by real-time NMR

For the determination of residue-specific oligomerization rate constants (k_{app}), a series of two dimensional ^{15}N–^{1}H HSQC spectra were recorded after oligomerization was directly initiated in the NMR tube at 37 °C by the addition of an appropriate volume of concentrated aggregation buffer such that the final buffer composition was 10 mM sodium acetate, 150 mM NaCl, and 10% D_2O (pH 4.0). The amide chemical shift assignments were retrieved from the NaCl titration experiments described in the previous section. By the end of the oligomerization reaction, resonances corresponding to the NTR residues, which had previously been shown to be dynamic in the oligomers by HX coupled to mass spectrometry (HX-MS) [27,28] and a small subset of CTD residues,

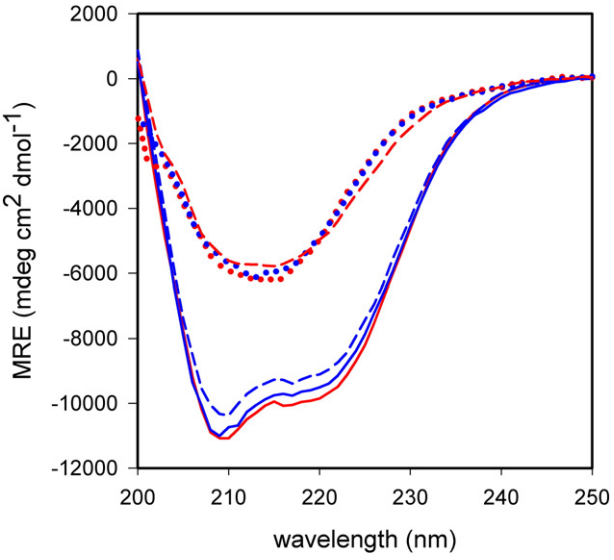

Fig. 3. Oligomerization of WT and E195K moPrP at pH 4 and 5.5. CD spectra of WT moPrP (solid blue line) and E195K moPrP (solid red line) at pH 4 in the absence of added salt; WT moPrP (dotted blue line) and E195K moPrP (dotted red line) after 24 h in oligomerization conditions (at pH 4 and 150 mM NaCl); WT moPrP (dashed blue line) and E195K moPrP (dashed red line) after 24 h in oligomerization conditions (at pH 5.5 and 150 mM NaCl). At pH 4, in the absence of salt, both proteins are monomeric and α-helical. At pH 4 and in 150 mM NaCl, both proteins form β-sheet-rich oligomers in 24 h. However, at pH 5.5 and in 150 mM NaCl, WT moPrP remains α-helical, whereas E195K moPrP has oligomerized completely in 24 h.

remained visible, while resonances from the rest of the CTD disappeared completely into the baseline (Fig. 5). This provided an excellent opportunity to probe residue-specific monomer-loss kinetics without any interference from signals from at least the core of the oligomers, which are expected to be broadened beyond detection at all times.

Addition of 150 mM NaCl attenuates NMR signal intensity by ~50%

Upon the addition of NaCl to initiate aggregation in the NMR tube, a uniform signal loss of ~50% amplitude was observed for all residues in the first spectrum, (Fig. S3), with negligible changes in line width (data not shown). Since highly conducting solutions like buffers containing high concentrations of salt are known to reduce the sensitivity of cryoprobes at high magnetic fields [58–60], it was important to establish if the apparent burst phase loss in signal was merely an effect of salt on the sensitivity of the experiment or a result of ~50% molecules undergoing instantaneous aggregation, leading to signal loss.

For this purpose, the following control experiments were carried out: (1) the apparent burst phase loss in signal was quantified at 50, 100, and 200 μM protein concentrations. For all isolated resonances, this apparent burst phase had negligible monomer concentration dependence (Fig. S3), confirming that the ~50% attenuation in signal during this time period was due to the reduced sensitivity of the cryoprobe in the presence of 150 mM NaCl. (2) Monomer-loss kinetics was also measured at pH 5.5 in the presence of 150 mM NaCl, where oligomerization has been shown to be extremely slow [23]. If the signal loss at the first kinetic time point was a result of loss in sensitivity due to salt, it could be expected to be observed at all pH values, as long as the salt concentration was kept fixed. Indeed, a comparable attenuation in signal was observed at pH 5.5, following which the signal remained constant, indicating that virtually no monomer loss took place in 24 h (Fig. S4). In addition, CSPs were also found to be

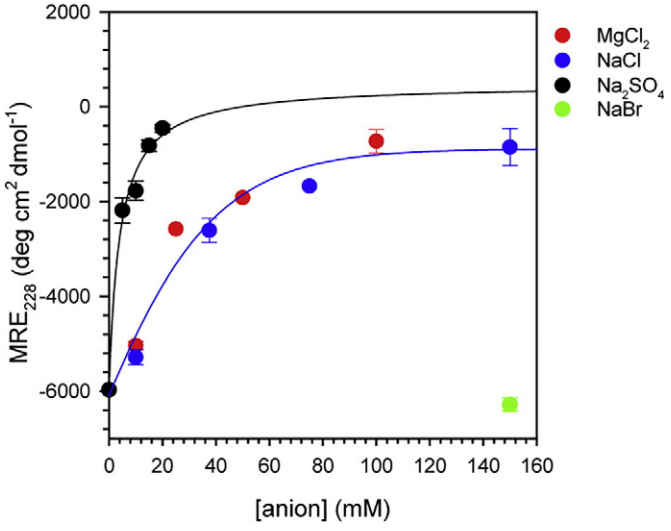

Fig. 4. Oligomerization of WT moPrP at pH 4 in different salts. Far-UV CD signal at 228 nm after 24 h of oligomerization in 5, 10, 15, and 20 mM of Na_2SO_4 (black); 5, 12.5, 25, and 50 mM of $MgCl_2$ (red); 10, 37.5, 75, and 150 mM of NaCl (blue); and 150 mM NaBr (green). In the case of $MgCl_2$, the chloride concentrations were therefore 10, 25, 50, and 100 mM. Solid lines through the data were drawn to guide the eye.

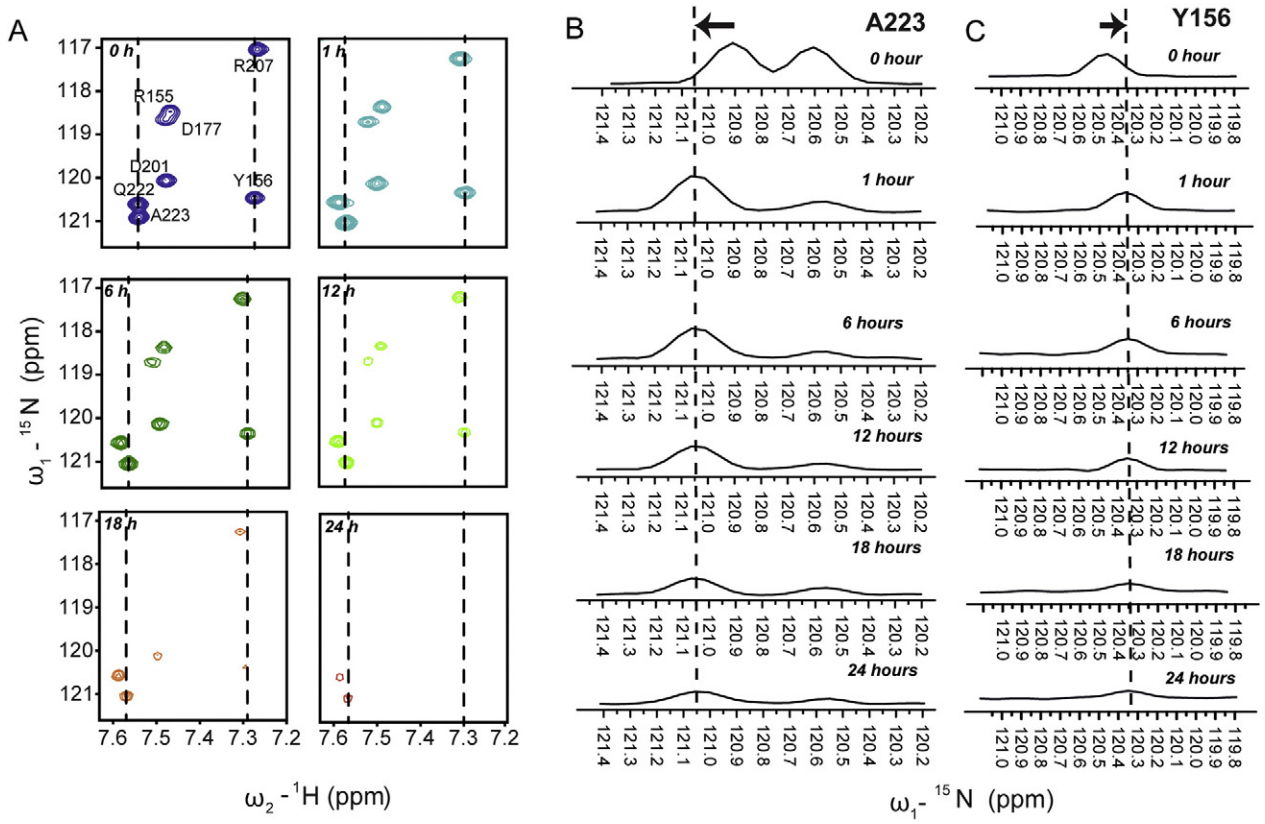

Fig. 5. Monomer-loss kinetics monitored by real-time NMR. (A) Small sections of ^{15}N–^{1}H HSQC spectra for 100 μM moPrP before and after 1, 6, 12, 18, and 24 h of oligomerization, initiated directly in the NMR tube at 37 °C. Most CTD residues have disappeared completely at 24 h, indicating that all monomer has converted into oligomer. The oligomer is invisible to solution NMR due to its large size and enhanced transverse relaxation rates resulting in broad lines. However, NTR residues remain visible after oligomerization is complete, indicating that the NTR is dynamic even in the oligomer. (B and C) Representative 1D ^{15}N slices taken at the cross-sections indicated by dashed lines in Fig. 3A for residues A223 and Y156. Arrows indicate the direction of peak movement immediately upon the addition of salt, and the dashed line indicates the shifted peak position. After 24 h of oligomerization, both peaks are almost indistinguishable from noise. The new peak position remains unchanged for the rest of the oligomerization reaction.

independent of monomer concentration (data not shown), indicating negligible aggregation during the acquisition of the first spectrum.

Determination of residue-specific oligomerization rate constants

A series of two-dimensional ^{15}N–^{1}H HSQC spectra were acquired at regular time intervals, while the oligomerization reaction progressed in the NMR tube (see Materials and Methods). Most CTD residues disappeared into the baseline by the end of the oligomerization reaction (Figs. 5 and 6A). Changes in chemical shifts observed immediately upon the addition of NaCl remained unchanged for the rest of the oligomerization reaction (Fig. 5B and C). For the peaks that remained above the baseline throughout the oligomerization reaction, the decrease in intensity was accompanied by an increase in line width, with comparable rates (Fig. 6B).

The experiment was carried out over a 10-fold range of initial protein concentrations: 25, 50, 100, 200, and 300 μM. At all protein concentrations and for all assigned residues, the normalized intensity *versus* time data was described well by a single exponential equation. Residue-specific apparent rate constants of oligomerization were obtained as described in the Materials and Methods section [Eq. (3), Fig. 7A, and SI Table 1].

Monomer-loss kinetics is concentration dependent

The residue-specific apparent rate constants, k_{app} (h^{-1}), obtained from single exponential fits of the data were dependent on protein concentration (Fig. 7), suggesting that monomer loss did not follow true first order kinetics [61]. It was found that there was little variation in the apparent rate constants across the protein, for both the 200 and 100 μM data sets.

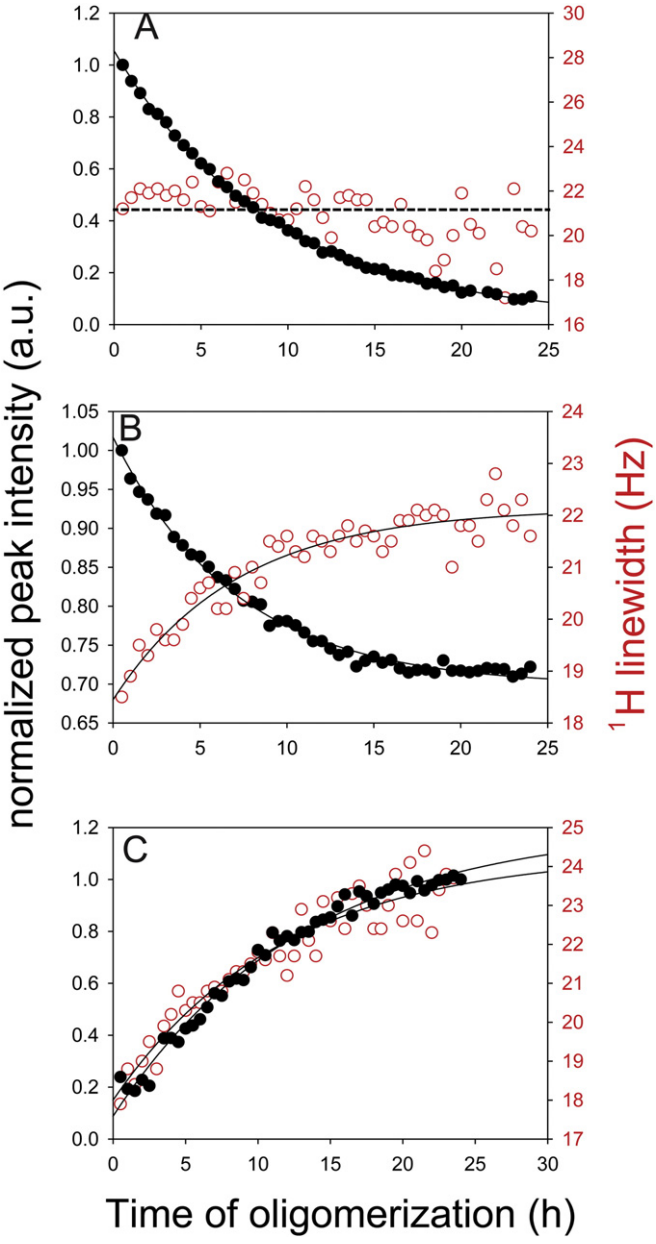

Fig. 6. Change in intensity and line width of representative resonances as a function of time. (A) Monomer-loss kinetics for representative CTD residue V121. The residue completely disappears by the end of the reaction. Monomer-loss kinetics is not accompanied by a change in line width. Most CTD residues follow this type of behavior. (B) Monomer-loss kinetics for representative residue G29. G29 remains visible throughout the oligomerization reaction. Only ~30% loss in intensity takes place by the end of the reaction. The reaction is accompanied by an increase in line width. (C) Representative peak from oligomeric species growing with time at a rate comparable to that of monomer disappearance. The increase in intensity is accompanied by an increase in line width. In panels (A and B), the peak intensities have been normalized to a value of 1 for the peak intensity in the first recorded spectra of aggregating protein.

However, for the 50 μM data set, the apparent rate constants were slightly higher for the NTR residues than for the CTD residues. The reason behind this difference is not understood at the present time.

Reaction order with respect to monomer concentration

The determination of reaction order with respect to monomer concentration (from monomer-loss kinetics) allowed the delineation of the rate-limiting step in aggregation reactions. For this purpose, reaction orders from initial rates [Eqs. (4) and (5)] were determined for each non-overlapping assigned residue [62–64].

Figure 8A represents the determination of normalized initial rate (v_0/C_0) for four representative residues N32, T94, V121, and A223. It is evident from the normalized data that the signal change for the NTR residues is considerably smaller than for the CTD residues. As a result, the initial rates (v_0), which are derived from the slope of the initial 10–25% of data, are systematically lower for the NTR residues as compared to the CTD residues (Fig. 8A). This apparent difference is eliminated if the initial rates are derived from a fractional plot, where the signal

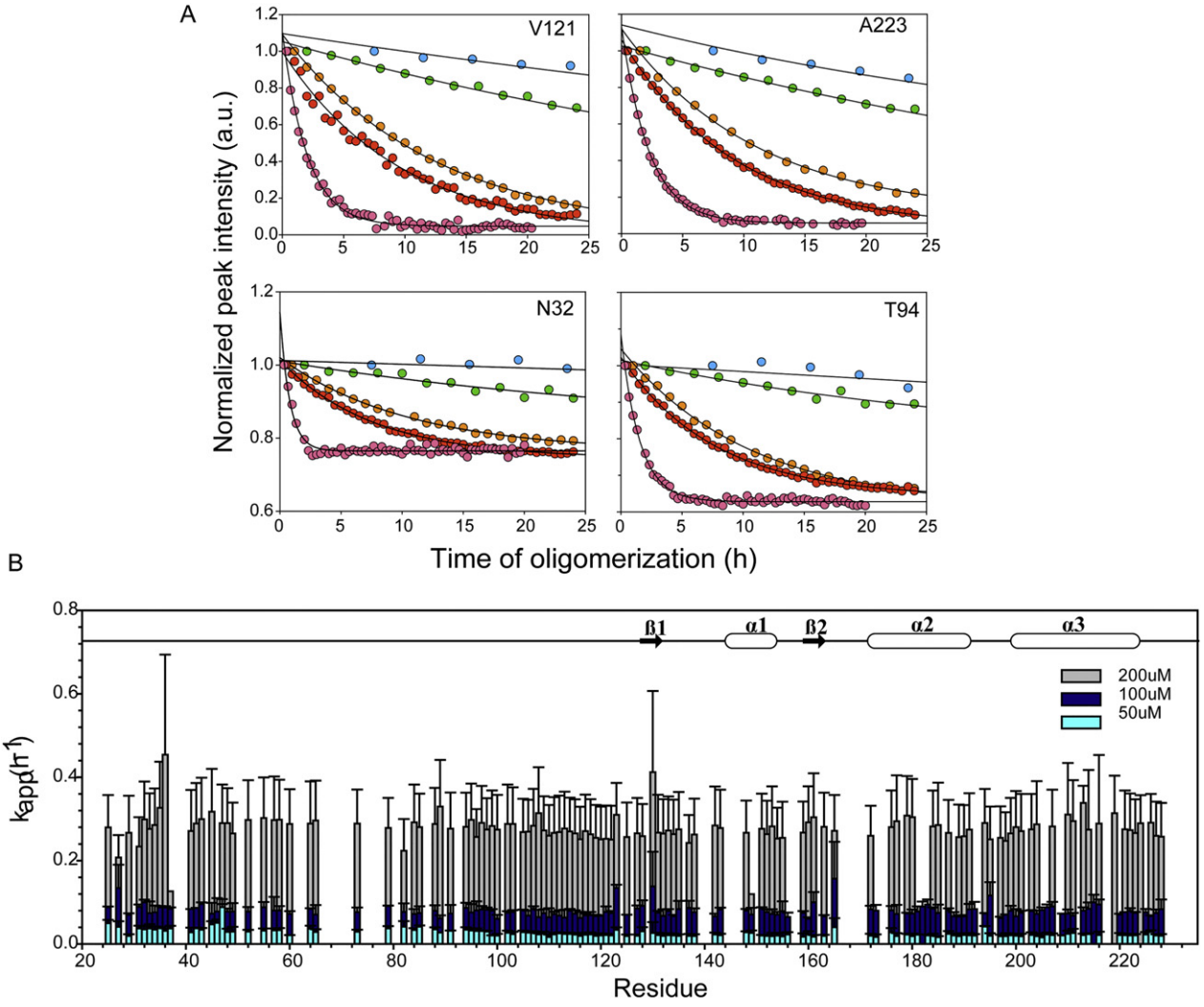

Fig. 7. Concentration dependence of monomer-loss rates monitored by real-time NMR. (A) Normalized peak intensity as a function of time for 300 (pink), 200 (red), 100 (orange), 50 (green), and 25 (light blue) μM moPrP for four representative residues V121, A223, N32, and T94. Each decay curve was fit to a single exponential equation to obtain an apparent rate constant, k_{app} (h^{-1}), for every assigned residue. The fit through the data is shown by the black line. (B) Residue-specific rate constants k_{app} (h^{-1}) for 50 (light blue bars), 100 (blue bars), and 200 (gray bars) μM protein concentrations for all assigned residues (SI Table 1). Overlapping and unassigned peaks have been excluded from the analysis. The error bars are obtained from two independent experiments. Error bars indicate ±1 s.e. Data for the other concentrations have not been shown for the sake of clarity.

changes for both NTR and CTD residues are comparable, and scale between 0 and 1. This is seen clearly in Fig. S5. In addition, the initial rates, from Fig. S5, and rate constants reported in Fig. 7 and Table S1 are also similar. From the slope of log (v_0/C_0) *versus* log (C_0), the order was determined for all assigned residues, as depicted in Fig. 8B and C. The mean reaction order was found to be 2.6 ± 0.2.

Table 1. Comparison of average monomer loss and oligomer growth rates

Probe	Rate (h^{-1})		
	50 μM	100 μM	200 μM
Monomer loss (NMR)	0.03 ± 0.01	0.08 ± 0.03	0.28 ± 0.03
Oligomer growth (NMR)	0.02 ± 0.01	0.08 ± 0.02	0.20 ± 0.04

Appearance of new peaks from growing oligomer species

Four new resonances appeared during the course of the oligomerization reaction (Fig. S6 and Fig. S7). The rate at which the intensities of these resonances increased was comparable to the rate at which the intensities of monomer resonances decreased (Fig. 6 and Table 1). The increase in intensity of these resonances was coincident with an increase in line

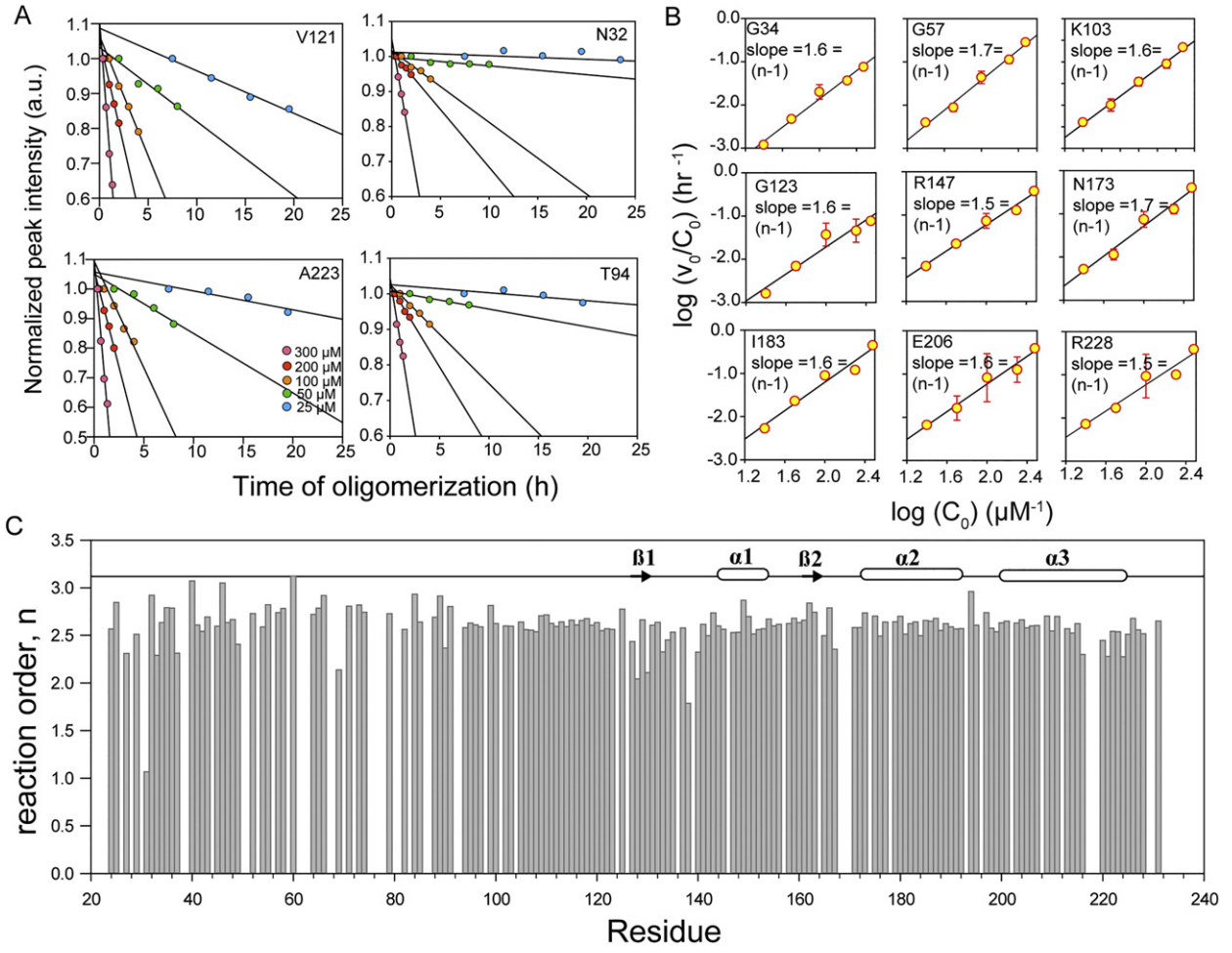

Fig. 8. Initial rate and order determination. (A) The initial rate was calculated from the slope obtained from the linear regression of the first 10–25% of normalized data for every concentration. (B) The logarithm of initial rate obtained in this manner was plotted against the logarithm of initial monomer concentration. From the slope of the linear regression of this log–log plot, $(n-1)$ was determined, where n is the order of the reaction. (C) Reaction order, n with respect to monomer plotted for every assigned residue. The mean order was determined to be 2.6 ± 0.2.

width (Fig. 6C), indicating that the species, to which these resonances belonged, was growing in size as time progressed. The rate at which the intensity of these resonances increased was also dependent on the monomer concentration, indicating that they were indeed reporting on an oligomerization reaction (Fig. S7C) concomitant with the monomer-loss kinetics.

Salt dependence of the initial rates of oligomerization

In order to evaluate the effect of salt on the association of monomers during oligomerization, initial rates of monomer loss were measured for a fixed protein concentration of 100 μM and a range of sodium chloride concentrations. For all assigned and non-overlapping residues, the initial rates of oligomerization were found to be directly proportional to the salt concentration (Fig. 9 and Fig. S8). The Debye–Hückel [65] charge screening effect was further established from the observation that the dependence of log (rates) on $\sqrt{I}$ was linear. This indicated that salt affects oligomerization in a non-specific manner by screening the significant positive charge on the monomers at pH 4, thereby aiding in the association reaction. In the absence of salt, oligomerization is predicted to be very slow but not entirely abolished.

Discussion

Salt causes a major perturbation in and around the K193–E195 salt bridge and minor perturbations throughout the monomeric protein

The prion protein is prone to misfolding under acidic conditions. Previous studies aimed at understanding

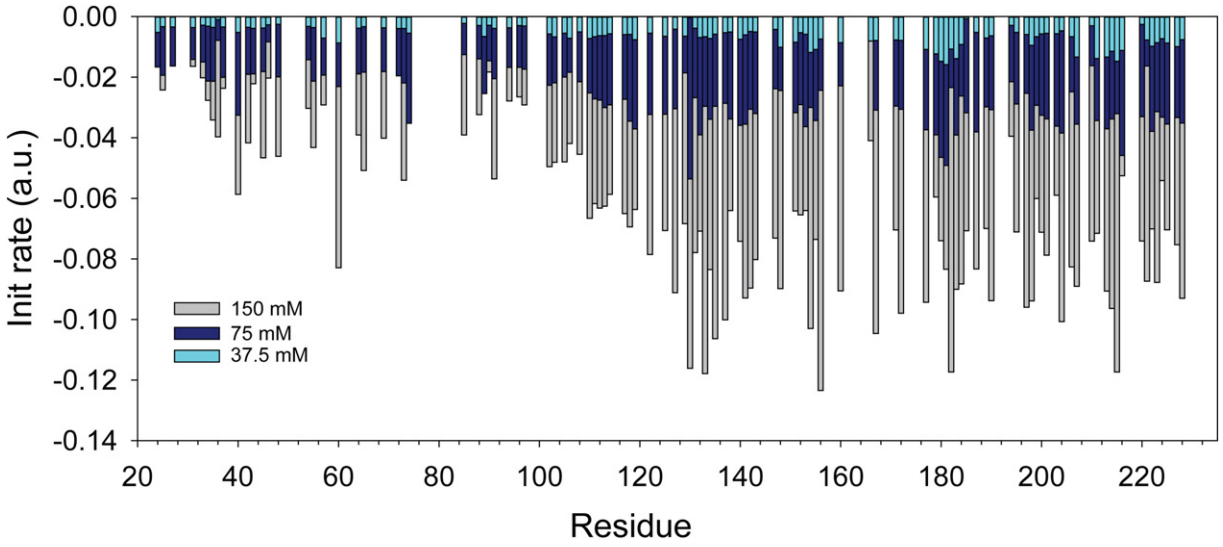

Fig. 9. Dependence of the initial rates of monomer-loss kinetics on salt concentration. Residue-specific initial rates of monomer loss for 100 μM moPrP for 37.5 (cyan bars), 75 (blue bars), and 150 (gray bars) mM NaCl concentrations for all assigned residues. A significant effect of salt concentration on oligomerization is evident from the initial rates of monomer loss. Overlapping and unassigned peaks have been excluded from analysis.

the effect of acidic pH and charge-reversing mutations, some of which are associated with disease, have established that the protonation of critical residues is responsible for the destabilization of the monomeric prion protein leading to its misfolding and oligomerization [66–69,48,49,70,71,26]. Specifically, at pH 4, protonation of residues H186 and D201 was identified to be critical in the misfolding process due to the disruption of electrostatic interactions between residues R155, H186, E195, and D201, resulting in the separation of the α1-β1-β2 and α2-α3 subdomains in monomeric moPrP [49,72,26]. This is corroborated by the extremely slow oligomerization rates of moPrP at pH 5.5 (Fig. 3 and Fig. S4) as compared to pH 4 in the presence of 150 mM NaCl [23]. Consequently, in the pathogenic mutant variants H186R and E195K, significant destabilization of the monomeric protein and accelerated misfolding and oligomerization were observed, probably due to the disruption of the same electrostatic network [49,72,26]. In supporting these observations, both kinetic and equilibrium experiments have reported intermediates with α1 unfolded and detached from the α2-α3 subdomain [73,74,23,27].

While the protonation of critical residues by a lowering of pH is necessary for the misfolding and oligomerization of moPrP, the presence of salt appears to be absolutely essential. In the absence of salt, moPrP does not misfold and oligomerize in an experimentally tractable timescale at pH 4. Binding and screening electrostatic interactions in proteins by salt are operative in the low salt concentration regime, while hydrophobic interactions are perturbed, or water structure around the protein molecules is altered only by high concentrations of salt. Thus, at pH 4 and in 150 mM NaCl, specific anion binding and salt-induced screening of electrostatic interactions in the monomeric protein (see below) appear to be critical in triggering misfolding and oligomerization.

In this study, the NaCl titrations of the CSPs were suggestive of ion binding to the protein (Fig. 1). However, the modest magnitudes of CSPs along with the millimolar range of NaCl concentrations required for their manifestation suggest that the binding is very weak, and that the salt-bound form (M*) is almost native-like. This was confirmed by CD spectra where no drastic conformational changes were observed immediately after the addition of salt (Fig. S2).

At pH 4 in the absence of salt, the protein is predominantly native and populates the unfolded state to $<0.05\%$ [23]. Even under oligomerization conditions, that is, in the presence of salt, the population of the unfolded state is too low to be detectable, as has been shown by kinetic HX-MS experiments [27]. Moreover, for both NTR mutant variants G113V and A116V, which are as stable as WT moPrP, the apparent rate constants of oligomerization are significantly faster than that of the WT protein. If oligomerization proceeded through the unfolded state, which is populated to the same extent for G113V, A116V, and WT moPrP, then all the proteins would have oligomerized with the same rate constants [27]. It is therefore unlikely that the oligomerization occurs through the denatured state.

The magnitudes of CSPs reported in this study are comparable to those reported for the binding of salt ions to the proteins Ltn and ephrin B2 [75], further reinforcing that the binding of NaCl to moPrP is weak

but specific. Since no new peaks appeared immediately upon the binding of salt, and line widths remain unchanged, the binding was in fast exchange. In addition, since the residues with the highest CSPs were distributed all over the protein, there appeared to be multiple dispersed binding sites.

When mapped onto the structure of moPrP, four of the eight most perturbed residues (T191, K193, G194, and E195) were found to lie in the loop between α2 and α3 in the monomeric protein. The rest of the perturbed residues (H60, V111, Q211, and K219) were dispersed all over the protein (Fig. 2B). The α2-α3 loop has previously been shown to be highly dynamic [76,77] and weakly protected in the monomer by NMR and HX-MS, respectively [27,28]. It seems that it is the disruption of the partially buried salt bridge between residues K193 and E195 that results in these localized perturbations (Fig. 2C). However, these perturbations did not affect the overall fold of the protein (Fig. S2), and the major conformational changes leading to the formation of the β-sheet-rich oligomers seem to occur later in the aggregation pathway.

In order to maintain favorable electrostatic interactions with residues R155 (positioned in the loop between α1 and β2) and K193 at pH 4, residue E195 is likely to have a depressed pKa, so that it is ionized at pH 4. Indeed, E195 has been reported to have a pKa of 2.09 [73]. pKa values of ionizable side chains are typically measured in NMR by monitoring the chemical shifts of the side-chain atoms while titrating the pH. For proteins, lengthy multidimensional experiments have to be carried out at high protein concentrations (~0.5 mM) to obtain pKa values of individual side chains [78,79]. In the case of moPrP, the protein at such high concentrations oligomerizes rapidly upon the addition of salt, and the monomer signal drops, reducing the signal-to-noise (S/N) in these lengthy experiments. Hence, due to technical difficulties, it was not possible to measure the pKa of E195 upon the addition of salt.

Interestingly, the charge-reversing pathogenic mutant variant E195K moPrP, with the disrupted K193–E195 salt bridge, readily undergoes misfolding and oligomerization at pH 5.5 in the presence of 150 mM NaCl, in contrast to WT moPrP. The placement of two positively charged residues K193 and K195 would result in repulsion in the α2-α3 loop in the pathogenic mutant, predisposing the protein to misfold, even at pH 5.5, where WT moPrP shows almost negligible misfolding and oligomerization (Fig. 3). Unfortunately, at pH 6 and above, the E195K mutant protein was found to precipitate, upon the initiation of oligomerization with 150 mM NaCl. This result substantiates an earlier study where a small chemical chaperone, GN8, was found to impede pathogenic conversion of the cellular prion protein by intercalating in a pocket created by residues N158, V188, T191, K193, and E195 and by inhibiting the disruption of the R155–K193–E195 salt-bridge network [80]. Together, these results suggest that the salt-binding-induced disruption of the key salt bridge between residues K193 and E195 in the loop between α2 and α3 in the monomer is the trigger for the salt-induced low-pH oligomerization of the prion protein.

It is interesting to note that kinetic HX-MS experiments carried out in the presence of salt for WT moPrP were unable to detect these salt-induced perturbations in the loop between α2 and α3 or residues H60 and V111 in the NTR, because these residues are highly dynamic and solvent-exposed in the monomer. In contrast, from HX-MS studies of pathogenic mutants G113V and A116V, dimer formation was shown to be driven by the palindromic region in the NTR of monomeric moPrP containing both these mutations [81,28]. The NTR in the WT oligomers remains dynamic and shows no change in solvent accessibility because either the mechanism of oligomerization or the structure of the WT oligomers is slightly different from the mutant oligomers. From this study, in WT moPrP, dimer formation seems to occur after salt binding perturbs the α2-α3 loop but is not detectable by solution NMR.

Equilibrium HX-MS experiments on both the WT and pathogenic mutants in the CTD of the monomeric moPrP have inferred that the steps through which misfolding and oligomerization commence include: (i) unraveling or unfolding of α1 followed by (ii) the exposure of the hydrophobic TVTTTT stretch at the C terminus of s finally culminating in the formation of β-sheet-rich oligomers. A general destabilization of α1 was observed for all pathogenic mutant proteins in their monomeric form regardless of the position and nature of the mutated residue [27]. In this study, none of the residues with significant CSP were found to lie in α1. The two possible explanations for this are: (i) α1 is destabilized in a minor alternate conformation of monomeric moPrP, which converts into oligomers upon the addition of salt, and (ii) perturbations in α1 occur only after the formation of higher-order structures invisible to NMR. The latter scenario is more probable because the rate at which α1 loses protection during the oligomerization of the WT protein monitored by kinetic HX-MS experiments is comparable to the overall oligomerization rate monitored by CD or size-exclusion chromatography [28].

Dual role of salt: specific binding and acceleration of monomer association by a non-specific screening effect

The oligomerization of the prion protein at acidic pH was found to be dependent on the nature of the anion but independent of the nature of the cation. Both $MgCl_2$ and NaCl were equally effective at inducing oligomerization (Fig. 4), at equivalent Cl^- concentrations. The observation that 20 mM SO_4^{2-}

induced the same extent of oligomerization as did 150 mM Cl^-, and that 150 mM Br^- was unable to induce oligomerization suggests strongly that the charge screening effect of the anion at pH 4 occurs by specific binding of the anion to the positively charged protein. It is unlikely that at these low concentrations, hydrophobic interactions are perturbed. Instead, it appears that specific binding of certain anions to the protein occurs, which screens electrostatic interactions, which then triggers misfolding and oligomerization. Similar results were seen for worm-like fibril formation of WT moPrP at pH 2 [80].

While specific interactions of salt with the protein can initiate the misfolding process as is exemplified here by the disruption of the K193–E195 salt bridge, a general screening of like charges can aid in oligomerization. Indeed, chloride ions have been surmised to induce the aggregation of the prion protein [55,56]. Moreover, anion binding has been shown to influence the kinetics of β-oligomer and worm-like fibril formation at pH 2 [82]. Furthermore, the removal of NaCl from buffer was found to affect the protease resistance of PrP^{Sc} (scrapie) and change the size distribution of aggregates [83].

At pH 4, monomeric moPrP has a calculated overall charge of +27. Not surprisingly, therefore, in the absence of salt, oligomerization is very slow ($\sim 10^{-4}$ h^{-1}). Salt is thus needed to screen the electrostatic repulsion between monomers in order for monomer association to proceed. Indeed, the initial rates of oligomerization were found to be significantly affected by the concentration of NaCl in solution (Fig. 9 and Fig. S8). The dependence of monomer-loss kinetics on NaCl concentration was similar for all residues, indicating that this was a non-specific effect. For protein–protein association reactions, the association rate is predicted to vary exponentially with the square root of ionic strength when only Debye–Hückel charge screening effects are operative. The linear dependence of log (rates) with $\sqrt{I}$ (Fig. S8) confirms that a similar mechanism is operative during the oligomerization of moPrP.

A similar effect of salt on protein aggregation has been observed for the full-length moPrP at pH 2 [82], alpha synuclein fibrils [84], yeast prion [85], β2 microglobulin [86], glucagon [87], and Aβ40 fibrils [88]. Mutations that decrease the overall charge of the protein have also been shown to promote aggregation [89]. Screening by salt therefore appears to be a common mechanism of salt-promoted protein association reactions, especially when the protein is highly charged [90].

It is intriguing to speculate whether the salt-binding-induced disruption of the K193–E195 salt bridge, or the overall screening of like charges, is the driving force for moPrP oligomerization. According to the extrapolated values from Fig. S8, moPrP is expected to oligomerize at pH 4 in the absence of salt with a rate of $\sim 10^{-4}$ h^{-1}. It therefore appears that salt accelerates the association process but may not be absolutely essential to it. On the other hand, the disruption of the K193–E195 salt bridge by salt binding and electrostatic screening seems to be the trigger for the salt-induced low-pH misfolding and oligomerization of moPrP. This is in part supported by the observation of faster misfolding and oligomerization rates of the salt-bridge-disrupted pathogenic E195K moPrP as compared to WT moPrP, at pH 4 and pH 5.5 in the presence of 150 mM NaCl [72,26].

Detection of mobile residues in oligomers formed at pH 4 and in 150 mM NaCl

Dynamic regions of large oligomers can be visible to solution NMR even when the core regions are completely broadened beyond detection. This happens when the local flexibility of these regions leads to "motional narrowing" of resonances, obscuring the line broadening resulting from the global tumbling of the large oligomer [91,92]. Briefly, two classes of monomeric residues were identified from the real-time NMR data. The first class of residues, composed of most CTD residues, decays completely into the baseline and is undetectable by the end of oligomerization (Fig. 5). The single exponential decay in intensity for these residues is not accompanied by a change in line width (Fig. 6A). The second class of residues decays with comparable rates but remains visible throughout the oligomerization reaction. A small subset of CTD residues (G123, V165, S230, and S232) and all of the assigned NTR residues belong to this class (Fig. S7). Residues S230 and S232 are at the very end of the CTD of the monomeric protein, while residue G123 lies at the very beginning of the CTD. V165 lies in the loop between β2 and α2. All residues apart from V165 lie in sequence segments, which are solvent-exposed in the oligomer as probed by HX-MS [27,28]. The change in intensity for these residues is accompanied by an increase in line width, indicating that at all time points, both monomer and oligomer contribute to the signal, and these residues remain mobile in the oligomer (Fig. 6). For tau and IAPP fibrils, residues that displayed residual intensity in NMR spectra were shown to be directly correlated with their distance from the core of the fibril [93,94].

The rate constants at which the intensities of the NTR and CTD residues decay in the NMR experiments are on the same timescale as the kinetics of oligomerization probed by other methods like CD, size-exclusion chromatography, and HX-MS [27]. The end product of the oligomerization reaction is soluble β-sheet-rich oligomers of R_h ~16 nm (Fig. S1). No visible particulates appear during or at the end of the oligomerization reaction that could impact magnetic inhomogeneity and peak intensity. The line widths of

peaks corresponding to the CTD are constant during the oligomerization reaction (Fig. 6A), indicating that T2* is unaffected. The oligomers appear spherical in atomic force microscopy images [33].

Interestingly, the oligomers formed at pH 4 and in 150 mM NaCl have their NTR completely disordered and their core mostly confined to the CTD of the protein. This is in marked contrast to the brain-derived fibrillar aggregates, which have their core extended down to residues 80–90 in the NTR [37].

Oligomers continuously accumulate and increase in size with time

The single exponential nature of monomer-loss kinetics suggests that the monomer-to-oligomer conversion occurs in a single step. However, it is physically very improbable that the formation of *n*-mers with $n > 2$ or 3 will occur in a single step. In a multistep oligomerization reaction, multiple intermediates can get populated simultaneously or consecutively. However, the intermediate species in the oligomerization reaction will be invisible to solution NMR if they are large in size or low in population [95–97,61].

While the core residues of the oligomers, mostly constituted by the CTD, are completely invisible to solution NMR, due to their size and rigidity, dynamic residues in the oligomers that are in a conformation different from that in the monomer appear as new resonances in the NMR spectrum as oligomerization proceeds. Four such resonances, although unassigned, appeared and grew at a rate comparable to monomer-loss rates in a concentration-dependent manner (Figs. S6 and S7) with a concomitant increase in line width (Fig. 6 and Table 1).

It is unlikely that these new peaks are from lysine and arginine side chains, which appear at low pH and/or at high salt concentrations. Lysine and arginine side-chain peaks might appear immediately upon the addition of salt but are unlikely to grow in intensity as the oligomerization reaction proceeds with time. To further confirm that these are indeed new peaks, HSQC spectra of the monomer and oligomer were recorded with a longer sweep width to exclusively look for lysine/arginine side chains. Lysine side-chain peaks were not observed in either the monomer or the oligomer. No new arginine side-chain peaks were observed upon oligomerization. Some arginine side-chain peaks disappeared in the oligomer spectra similar to the backbone amide peaks (Fig. S7). Hence, the new peaks do not appear to be side-chain resonances.

Intriguingly, the four new resonances emerging from the dynamic regions of the oligomer are useful reporters of the oligomer species (Fig. S6). The intensities and line widths of these new peaks can serve as important NMR parameters to monitor oligomer population and size, respectively. While the increase in signal intensity indicated that the population of oligomers was growing as time progressed, the increase in line width indicated that the oligomeric species was simultaneously growing in size (Fig. 6C). The rate at which both intensity and line width increased for these resonances was comparable to the monomer-loss rates, indicating that they were monitoring the same process (Table 1). The increase in line width for residues belonging to the NTR confirmed the same. Together, these results suggest that all intermediate species that form as oligomerization proceeds contribute to the signal of these resonances at every kinetic time point.

The monomer-loss kinetics is limited by an association reaction and not by conformational change

The Lumry–Eyring mechanism [98] of protein aggregation posits that the reaction is initiated by a conformational change of the native protein (in most cases, unfolding) and proceeds by a series of bimolecular reactions [63,61]. Aggregate growth commences with dimer formation and continues either by the addition of monomers and/or by fusion of smaller oligomers (as small as a dimer) to form larger oligomers. Both dimer formation and its subsequent growth by the addition of monomers consume monomers and will lead to a signal loss in real-time NMR experiments. Fusion of smaller oligomers to form larger oligomers is not discernible to this probe due to size limitations. While the first step is a first-order conformational change, the subsequent steps are all higher order with respect to the monomer. The determination of reaction order with respect to the monomer can aid in identifying the rate-limiting step in the aggregation reaction.

For unfolding (conformational change)-limited protein aggregation reactions, monomer loss follows true single exponential kinetics with rate constants independent of protein concentration and a reaction order of ~1 [99,100]. Pseudo-first-order kinetics is generally observed when aggregate growth occurs by monomer addition. Indeed, monomer addition to seeds in fibril elongation experiments, where the elongation of fibrils does not change its concentration, appears as a pseudo-first-order reaction with a concentration-dependent rate constant [101]. Reaction orders greater than 1 with single exponential monomer-loss kinetics are observed for association- and rearrangement-limited aggregation reactions. In this study, the average reaction order across all assigned residues was determined to be 2.6 ± 0.2 (Fig. 8).

While the microscopic rate constants for each step are still unknown, the single exponential nature of monomer-loss kinetics, concentration-dependent apparent rate constants of monomer loss, and a mean reaction order across residues greater than 2 altogether indicate that the rate of prion protein oligomerization is limited by association. The rate-limiting step

in oligomerization was determined to be dimer formation in an earlier study with a reaction order of 2 [28]. A reaction order of 2.6 might be a result of multiple association reactions occurring simultaneously, in which either two or three monomers come together to form a dimer or a trimer. A similar reaction order of 2.5 was found previously for the aggregation of lactic dehydrogenase, which was believed to be the consequence of multiple rate-limiting steps [102]. It should, however, be kept in mind that the association of more than three molecules in the rate-limiting step is highly improbable. Our data are in qualitative agreement with an earlier combined Fourier Transform Infra-Red (FTIR) and CD study of the growth of oligomers from Syrian Hamster PrP90–232, which have also reported a reaction order of 3 [103]. In addition, an Atomic Force Microscopy (AFM) study on the oligomerization mechanism of WT and 10OR mutant variant of human prion protein reported that the first species sufficiently stable so as to be visible was composed of 3–4 monomers, following which growth occurred by fusion of these seeds and not monomer addition [104].

In marked contrast, in an earlier study of the oligomerization kinetics of the CTD of moPrP, reaction orders ranging from 5 to 40 were reported for different groups of residues [14]. However, this result was not obtained by the determination of the concentration dependence of oligomerization rates as was done in the current study. Instead, reaction orders were obtained by fitting kinetic data to an nth-order equation at a single protein concentration. Such analysis should be treated with caution as more than one set of values of rate constants and order can yield very similar quality of fits. Moreover, the size of the species (number of monomers) formed at each step was directly inferred from the reaction order for different sets of residues. The reaction orders thus obtained are not physically realistic.

The results of the current study clearly suggest that the mechanism of oligomer growth is critically dependent upon solvent conditions and the starting conformation of the monomeric protein. However, using simple kinetic analysis of data, it is possible to identify the rate-limiting step in a multistep complex pathway, thereby shedding light on the mechanism of protein oligomerization.

Conclusion

Real-time NMR experiments to probe the oligomerization kinetics of moPrP at pH 4 and 150 mM NaCl identify subtle structural perturbations in the monomeric protein preceding the major conformational changes that lead to misfolding and oligomerization. The results suggest that while low pH is needed for the protonation of critical residues in the monomeric prion protein, it is not sufficient to trigger misfolding and oligomerization in the absence of NaCl. NaCl binding to the monomeric protein causes major perturbations in the α2-α3 loop by disrupting the salt bridge between residues K193 and E195. However, the overall structure of the monomeric protein remains intact upon loop perturbation. These perturbations lead to conformational changes that act as a trigger for the subsequent misfolding and oligomerization of moPrP (Fig. 10).

The rate-limiting step in the oligomerization reaction is a higher-order association reaction with a mean reaction order of 2.6 across residues and not conformational change. Salt also accelerates the oligomerization reaction by screening the significant positive charge on the monomers at pH 4 (Fig. 9 and Fig. S8). The manifold effect of salt binding and electrostatic screening on the low-pH oligomerization of moPrP provides crucial insight into the oligomerization mechanism.

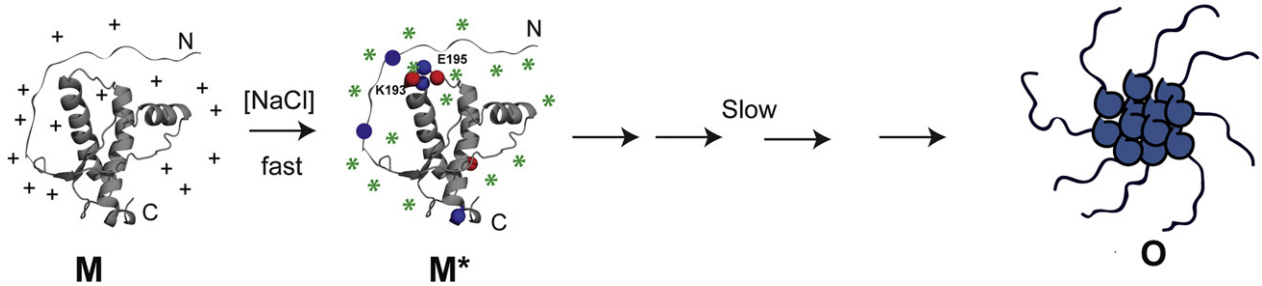

Fig. 10. Mechanism of salt-mediated low-pH oligomerization of the prion protein. The highly charged native protein (M), upon the addition of salt (green asterisks), immediately undergoes subtle perturbations (shown by blue and red spheres) and converts into native-like M*. A localized perturbation occurs in the loop between α2 and α3 in the vicinity of the K193–E195 salt bridge due to salt binding. The slower steps of misfolding and oligomerization then lead to the formation of the oligomer O, which is also facilitated by the electrostatic screening mechanism of salt. The NTR in oligomer O is disordered as it is in the native-state M.

Materials and Methods

Reagents

All reagents used for experiments were of the highest purity grade available from Sigma Aldrich unless otherwise specified. Reagents used for the protein preparation were from HiMedia and Fisher Scientific.

Protein expression and purification

The full length, recombinant moPrP encoded in the pET-17b(+) plasmid was transformed into *Escherichia coli* BL21(DE3) codon plus (Stratagene) cells. A single colony was used to inoculate 25 ml of LB media containing 100 μg/ml ampicillin and was grown at 37 °C for 8 h. A 50-μL aliquot of this primary culture was used to inoculate 50 ml of M9 minimal media containing 1 g/L $^{15}NH_4Cl$ and 3 g/L ^{12}C-glucose (or ^{13}C-glucose) and was grown overnight. This was further used to inoculate 1 L of ^{15}N or $^{15}N/^{13}C$-labeled M9 media and was grown for 5–6 h until it reached an OD_{600} = 1.8–2, when protein expression was induced using IPTG at a final concentration of 0.4 mM. The cells were allowed to grow for an additional 12 h before harvesting and further purification. ^{15}N or $^{15}N/^{13}C$-labeled prion protein was purified and stored in 10 mM sodium acetate, pH 4 at −80 °C as described previously [23]. The E195K mutant variant of moPrP was purified in the same way as described previously [27]. The purity of the protein(s) was confirmed using mass spectrometry.

Far-UV CD and Dynamic Light Scattering (DLS) measurements

All CD and Dynamic Light Scattering (DLS) measurements were carried out as described previously [28]. The protein concentration used for all oligomerization experiments was 100 μM. For the CD measurements, the protein was diluted to 10 μM in the appropriate buffer, just before measurement.

Solution-state NMR spectroscopy

NMR backbone resonance assignment for moPrP(23–231)

A ^{13}C, ^{15}N-labeled moPrP sample at a concentration of 0.5 mM in 90% H_2O/10% D_2O (v/v) at pH 4, 10 mM sodium acetate buffer was used for NMR backbone resonance assignments. All the backbone resonance assignment experiments were carried out at 310 K on an 800 MHz Bruker Avance spectrometer equipped with a cryo-probe. The following NMR experiments were recorded: 2D ^1H–^{15}N HSQC, 3D HNCO, 3D HN(CA)CO, 3D HNCA, 3D HN(CO)CA, 3D HNCACB, and 3D CBCA(CO)NH. The data were processed in NMRPipe [105] and analyzed in Sparky (T.D. Goddard and D.G. Kneller, SPARKY 3, University of California, San Francisco). The resonance peaks observed in the recorded data set were submitted to the PINE [106] server for an initial round of automated backbone resonance assignments. Finally, all resonance assignments were assigned and confirmed manually. A secondary structure prediction was carried out using the H^N, N, C^α, C^β, and C′ chemical shift values by TALOS+ [107]. The predicted secondary structure agreed with the three-dimensional structure of moPrP.

Monomer-loss kinetics monitored by real-time NMR

All NMR measurements were carried out at 37 °C. A reference spectrum in the absence of salt was collected before starting the real-time NMR measurements using the same parameters as for the kinetics experiment for every protein concentration. Oligomerization was initiated by the addition of 30 μL of 10× aggregation buffer (2× for 300 μM) to the protein, such that the final buffer composition was 10 mM sodium acetate, 150 mM NaCl, 10% D_2O at pH 4.0 in a total volume of 300 μL. After a dead time of ~10 min, acquisition was started. The same experiment was repeated for protein concentrations of 25, 50, 100, 200, and 300 μM, but with a different number of scans in each case in order to get reasonable S/N ratios for each data set. At high protein concentrations, where S/N ratios were better, but oligomerization kinetics was faster, higher sampling rates were employed, with each spectrum acquired with a fewer number of scans. However, at low protein concentrations, oligomerization rates were slower, but the S/N ratio was poor, so each spectrum was acquired with a higher number of scans, which finally resulted in slower sampling rates but better quality data. Typically, one HSQC experiment was recorded with 2048 points in the t_2 dimension and 256 increments in the t_1 dimension. Thus, for the 25 μM protein concentration, the acquisition time for each spectrum was ~4 h (48 scans), whereas for the 300 μM protein concentration, it was ~20 min (4 scans). All real-time NMR data sets were processed using NMRPipe using the same processing parameters [105] and analyzed with Sparky (T.D. Goddard and D.G. Kneller, SPARKY 3, University of California, San Francisco).

2D ^1H–^{15}N HSQC spectra with longer sweep width

To verify that the new peaks that appear during oligomerization are not from lysine or arginine side chains, 2D ^1H–^{15}N HSQC of 100 μM WT moPrP

monomer and oligomer with a longer sweep width were recorded. All parameters were kept the same as the earlier experiments, except the sweep width, which was fixed at 100 ppm in the F1 dimension for these measurements.

NaCl titration

In order to transfer assignments for the protein under native conditions to the protein in 150 mM NaCl, a NaCl titration was performed. A series of samples were prepared, keeping the protein concentration fixed at 100 μM, and the NaCl concentration was varied from 0 to 200 mM in 25-mM increments. Since the addition of NaCl at pH 4 causes the protein to oligomerize, 2× aggregation buffer containing the appropriate amount of NaCl was added to the sample just before the HSQC spectrum was acquired. Each spectrum was acquired for ~1 h, during which only ~5% oligomerization took place, in accordance with the rates obtained from the kinetic experiment for 100 μM protein.

The same data were used to obtain binding curves for protein–NaCl binding for all assigned residues. To probe the effect of salt on intensity, the intensity for each residue was normalized according to the formula (for every protein concentration):

$$\text{Normalized peak intensity} = \frac{I_s - I_s^b}{I_0 - I_0^b} \quad (1)$$

where I_s and I_0 are residue-specific intensities at 150 mM and 0 mM NaCl concentrations, respectively, and I_s^b and I_0^b are the corresponding spectral base lines estimated from Sparky.

CSPs were calculated according to the following formula:

$$\Delta\delta_{NH} = \sqrt{(\Delta\delta_H)^2 + \left(\frac{\Delta\delta_N}{5}\right)^2} \quad (2)$$

where $\Delta\delta_{NH}$ is the combined CSP in ppm, and $\Delta\delta_H$ and $\Delta\delta_N$ are the ^{1}H and ^{15}N chemical shift differences, respectively, between the native protein spectrum and the spectrum at each NaCl concentration.

Data analysis

The misfolding and oligomerization reactions were initiated in the NMR tube as described previously. For each data set, the intensity at each time point for each residue was normalized to the intensity of the first kinetic time point, I_1 according to:

$$\text{Normalized peak intensity} = \frac{I_t - I_t^b}{I_1 - I_t^b} \quad (3)$$

where I_t corresponds to the raw signal intensity at time t, I_t^b corresponds to the baseline (estimated from Sparky) for each spectrum at time t, and I_1 corresponds to the raw signal intensity at the first time point. It is to be noted that the first kinetic time point was used to normalize the data, and not the signal at $t = 0$, that is, in the absence of salt.

This was done; as upon the addition of salt, a significant but uniform decrease in intensity (~50%) was observed for almost all residues. This was due to the decreased sensitivity of the cryoprobe in the presence of salt (see Results). In addition, normalization taking the baseline into account ensured that the rate determination for all residues was not affected by their variable S/N ratios. Normalized peak intensities were plotted as a function of time and fit to a single exponential equation to obtain residue-specific apparent rate constants (k_{app}).

Monomer-loss kinetics was also monitored at pH 5.5 in the presence of 150 mM NaCl, where oligomerization kinetics is known to be extremely slow. For this purpose, the ^{15}N-labeled protein, initially in 10 mM sodium acetate (pH 4.0), was dialyzed against Milli-Q® water and then buffer exchanged into 20 mM Mes (pH 5.5). A reference spectrum was acquired before the addition of salt. The buffer composition after the addition of 2× aggregation buffer was 20 mM Mes, 150 mM NaCl, and 10% D_2O (pH 5.5).

Determination of line widths for isolated resonances

The ^{1}H line widths were estimated from the full width at half-maximum obtained by fitting isolated resonances to Gaussian functions using the built-in integration option in the Sparky software.

Determination of residue-specific initial rate and reaction order for the monomeric prion protein

For initial rate determination, the first 10–25% of the normalized data for each protein concentration was fit to a straight line, the slope of which was the initial rate per unit concentration (v_0/C_0) [63,62]. For an nth order reaction, the rate of monomer loss is described by

$$-\frac{dC}{dt} = k[C]^n \quad (4)$$

where C is the monomer concentration, k is the rate constant, and n is the order of the reaction.

Now, initial rate = $v_0 = -\frac{d[C]}{dt}\big|_{t=0} = k[C_0]^n$, where C_0 is the initial protein concentration. Since the data are normalized with respect to the signal for initial monomer concentration, the above equation becomes:

$$\frac{v_0}{C_0} = k[C_0]^{n-1}$$

Taking the logarithm on both sides,

$$log\left(\frac{v_0}{C_0}\right) = log\ (k) + (n-1)\ log\ C_0 \quad (5)$$

The slope of a linear fit of log (v_0/C_0) *versus* log (C_0) is equal to $n-1$, where n is the true reaction order with respect to monomer concentration.

Salt dependence of initial rates

The initial rates of monomer loss (as described above) were calculated for the oligomerization reactions of 100 μM protein at NaCl concentrations of 37.5, 75, and 150 mM. The dependence of initial rates of monomer loss at a fixed protein concentration and varying NaCl concentration provides a measure of the effect of salt on oligomerization kinetics.

Accession numbers

The chemical shifts have been deposited at the Biological Magnetic Resonance Bank, under accession code 26958.

Acknowledgments

We thank members of our laboratory for discussions. This work was funded by the Tata Institute of Fundamental Research and by the Department of Biotechnology, Government of India. I.S. is a recipient of the Innovative Young Biotechnologist Award (IYBA) 2013 from the Department of Biotechnology, Government of India. The NMR experiments were carried out at the NMR facility, National Centre for Biological Sciences. R.D. acknowledges a Ramalingaswami fellowship from the Department of Biotechnology, India. J.B.U is a recipient of a J.C. Bose National Fellowship from the Government of India.

Appendix A. Supplementary Data

Supplementary data to this article can be found online at http://dx.doi.org/10.1016/j.jmb.2017.05.006.

Received 7 December 2016;
Received in revised form 5 May 2017;
Accepted 7 May 2017
Available online 11 May 2017

Keywords:
prion oligomerization;
salt-binding;
K193–E195 salt bridge;
reaction order;
association-limited

Abbreviations used:
moPrP, mouse prion protein; CTD, C-terminal domain; NTR, N-terminal region; α1, alpha helix 1; β2, beta-strand 2; α2, alpha helix 2; α3, alpha helix 3; HX, hydrogen-exchange; HSQC, heteronuclear single quantum coherence; CSP, chemical shift perturbation; HX-MS, HX coupled to mass spectrometry; S/N, signal-to-noise.

References

[1] J.S. Griffith, Nature of the scrapie agent: self-replication and scrapie, Nature 215 (1967) 1043–1044, http://dx.doi.org/10.1038/2151043a0.
[2] S.B. Prusiner, Novel proteinaceous infectious particles cause scrapie, Science 216 (1982) 136–144.
[3] J. Castilla, P. Saa, C. Hetz, C. Soto, *In vitro* generation of infectious scrapie prions, Cell 121 (2005) 195–206, http://dx.doi.org/10.1016/j.cell.2005.02.011.
[4] G. Legname, Synthetic mammalian prions, Science 305 (2004) 673–676, http://dx.doi.org/10.1126/science.1100195.
[5] I.V. Baskakov, The reconstitution of mammalian prion infectivity de novo, FEBS J. 274 (2007) 576–587, http://dx.doi.org/10.1111/j.1742-4658.2007.05630.x.
[6] F. Wang, X. Wang, C.-G. Yuan, J. Ma, Generating a prion with bacterially expressed recombinant prion protein, Science 327 (2010) 1132–1135, http://dx.doi.org/10.1126/science.1183748.
[7] F. Wang, X. Wang, J. Ma, Conversion of bacterially expressed recombinant prion protein, Methods 53 (2011) 208–213, http://dx.doi.org/10.1016/j.ymeth.2010.12.013.
[8] S. Simoneau, H. Rezaei, N. Salès, G. Kaiser-Schulz, M. Lefebvre-Roque, C. Vidal, J.G. Fournier, J. Comte, F. Wopfner, J. Grosclaude, H. Schätzl, C.I. Lasmézas, *In vitro* and *in vivo* neurotoxicity of prion protein oligomers, PLoS Pathog. 3 (2007) 1175–1186, http://dx.doi.org/10.1371/journal.ppat.0030125.
[9] P. Huang, F. Lian, Y. Wen, C. Guo, D. Lin, Prion protein oligomer and its neurotoxicity, Acta Biochim. Biophys. Sin. 45 (2013) 442–451, http://dx.doi.org/10.1093/abbs/gmt037.Advance.
[10] B. Chesebro, Anchorless prion protein results in infectious amyloid disease without clinical scrapie, Science 308 (2005) 1435–1439, http://dx.doi.org/10.1126/science.1110837.
[11] P. Piccardo, J.C. Manson, D. King, B. Ghetti, R.M. Barron, Accumulation of prion protein in the brain that is not associated with transmissible disease, Proc. Natl. Acad. Sci. U. S. A. 104 (2007) 4712–4717, http://dx.doi.org/10.1073/pnas.0609241104.
[12] J.R. Silveira, G.J. Raymond, A.G. Hughson, R.E. Race, V.L. Sim, S.F. Hayes, B. Caughey, The most infectious prion protein particles, Nature 437 (2005) 257–261, http://dx.doi.org/10.1038/nature03989.
[13] K.J. Knaus, M. Morillas, W. Swietnicki, M. Malone, W.K. Surewicz, V.C. Yee, Crystal structure of the human prion protein reveals a mechanism for oligomerization, Nat. Struct. Biol. 8 (2001) 770–774, http://dx.doi.org/10.1038/nsb0901-770.
[14] K. Schlepckow, H. Schwalbe, Molecular mechanism of prion protein oligomerization at atomic resolution, Angew. Chem. Int. Ed. 52 (2013) 10,002–10,005, http://dx.doi.org/10.1002/anie.201305184.

[15] J. Singh, J.B. Udgaonkar, Molecular mechanism of the misfolding and oligomerization of the prion protein: current understanding and its implications, Biochemistry 54 (2015) 4431–4442, http://dx.doi.org/10.1021/acs.biochem.5b00605.
[16] C. Yang, W.L. Lo, Y.H. Kuo, J.C. Sang, C.Y. Lee, Y.W. Chiang, R.P.Y. Chen, Revealing structural changes of prion protein during conversion from alpha-helical monomer to beta-oligomers by means of ESR and nanochannel encapsulation, ACS Chem. Biol. 10 (2015) 493–501, http://dx.doi.org/10.1021/cb500765e.
[17] G.S. Jackson, A.F. Hill, C. Joseph, L. Hosszu, A. Power, J.P. Waltho, A.R. Clarke, J. Collinge, Multiple folding pathways for heterologously expressed human prion protein, Biochim. Biophys. Acta 1431 (1999) 1–13.
[18] G.S. Jackson, L.L.P. Hosszu, A. Power, A.F. Hill, J. Kenney, H. Saibil, C.J. Craven, J.P. Waltho, A.R. Clarke, J. Collinge, Reversible conversion of monomeric human prion protein between native and fibrilogenic conformations, Science 283 (1999) 1935–1937, http://dx.doi.org/10.1126/science.283.5409.1935.
[19] K. Jansen, O. Schafer, E. Birkmann, K. Post, H. Serban, S.B. Prusiner, D. Riesner, Structural intermediates in the putative pathway from the cellular prion protein to the pathogenic form, Biol. Chem. 382 (2001) 683–691, http://dx.doi.org/10.1515/BC.2001.081.
[20] L.L.P. Hosszu, M.A. Wells, G.S. Jackson, S. Jones, M. Batchelor, A.R. Clarke, C.J. Craven, J.P. Waltho, J. Collinge, Definable equilibrium states in the folding of human prion protein, Biochemistry 44 (2005) 16,649–16,657, http://dx.doi.org/10.1021/bi051277k.
[21] L.L.P. Hosszu, C.R. Trevitt, S. Jones, M. Batchelor, D.J. Scott, G.S. Jackson, J. Collinge, J.P. Waltho, A.R. Clarke, Conformational properties of beta-PrP, J. Biol. Chem. 284 (2009) 21,981–21,990, http://dx.doi.org/10.1074/jbc.M809173200.
[22] T. Hart, L.L.P. Hosszu, C.R. Trevitt, G.S. Jackson, J.P. Waltho, J. Collinge, A.R. Clarke, Folding kinetics of the human prion protein probed by temperature jump, Proc. Natl. Acad. Sci. U. S. A. 106 (2009) 5651–5656, http://dx.doi.org/10.1073/pnas.0811457106.
[23] R. Moulick, R. Das, J.B. Udgaonkar, Partially unfolded forms of the prion protein populated under misfolding-promoting conditions, J. Biol. Chem. 290 (2015) 25,227–25,240, http://dx.doi.org/10.1074/jbc.M115.677575.
[24] I.V. Baskakov, G. Legname, M.A. Baldwin, S.B. Prusiner, F.E. Cohen, Pathway complexity of prion protein assembly into amyloid, J. Biol. Chem. 277 (2002) 21,140–21,148, http://dx.doi.org/10.1074/jbc.M111402200.
[25] J. Singh, H. Kumar, A.T. Sabareesan, J.B. Udgaonkar, Rational stabilization of helix 2 of the prion protein prevents its misfolding and oligomerization, J. Am. Chem. Soc. 136 (2014) 16,704–16,707, http://dx.doi.org/10.1021/ja510964t.
[26] J. Singh, J.B. Udgaonkar, Unraveling the molecular mechanism of pH-induced misfolding and oligomerization of the prion protein, J. Mol. Biol. 428 (2016) 1345–1355, http://dx.doi.org/10.1021/acs.biochem.5b00605.
[27] J. Singh, J.B. Udgaonkar, Structural effects of multiple pathogenic mutations suggest a model for the initiation of misfolding of the prion protein, Angew. Chem. Int. Ed. 54 (26) (2015) 7529–7533, http://dx.doi.org/10.1002/anie.201501011.
[28] A.T. Sabareesan, J.B. Udgaonkar, Pathogenic mutations within the disordered palindromic region of the prion protein induce structure therein and accelerate the formation of misfolded oligomers, J. Mol. Biol. 120 (2016) 3935–3947, http://dx.doi.org/10.1016/j.jmb.2016.08.015.
[29] D.R. Borchelt, A. Taraboulos, S.B. Prusiner, Evidence for synthesis of scrapie prion proteins in the endocytic pathway, J. Biol. Chem. 267 (1992) 16,188–16,199.
[30] J.E. Arnold, C. Tipler, L. Laszlo, J. Hope, M. Landon, P.R.J. Mayer, The abnormal isoform of the prion protein accumulates in late-endosome-like organelles in scrapie-infected mouse brainitle, J. Pathol. 176 (1995) 403–411.
[31] C. Sunyach, A. Jen, J. Deng, K.T. Fitzgerald, Y. Frobert, J. Grassi, M.W. Mccaffrey, R. Morris, The mechanism of internalization of glycosylphosphatidylinositol-anchored prion protein, EMBO J. 22 (2003) 3591–3601.
[32] M.Q. Khan, B. Sweeting, V.K. Mulligan, P.E. Arslan, N.R. Cashman, E.F. Pai, A. Chakrabartty, Prion disease susceptibility is affected by beta-structure folding propensity and local side-chain interactions in PrP, Proc. Natl. Acad. Sci. U. S. A. 107 (2010) 19,808–19,813, http://dx.doi.org/10.1073/pnas.1005267107.
[33] J. Singh, A.T. Sabareesan, M.K. Mathew, J.B. Udgaonkar, Development of the structural core and of conformational heterogeneity during the conversion of oligomers of the mouse prion protein to worm-like amyloid fibrils, J. Mol. Biol. 423 (2012) 217–231, http://dx.doi.org/10.1016/j.jmb.2012.06.040.
[34] M. Kristiansen, P. Deriziotis, D.E. Dimcheff, G.S. Jackson, H. Ovaa, H. Naumann, A.R. Clarke, F.W.B. van Leeuwen, V. Menendez-Benito, N.P. Dantuma, J.L. Portis, J. Collinge, S.J. Tabrizi, Disease-associated prion protein oligomers inhibit the 26S proteasome, Mol. Cell 26 (2007) 175–188, http://dx.doi.org/10.1016/j.molcel.2007.04.001.
[35] B. Caughey, G. Baron, C. Bruce, M. Jeffrey, Getting a grip on prions:oligomers, amyloids, and pathological membrane interactions, Annu. Rev. Biochem. 78 (2009) 177–204, http://dx.doi.org/10.1146/annurev.biochem.78.082907.145410.
[36] F. Eghiaian, T. Daubenfeld, Y. Quenet, M. van Audenhaege, A.-P. Bouin, G. van der Rest, J. Grosclaude, H. Rezaei, Diversity in prion protein oligomerization pathways results from domain expansion as revealed by hydrogen/deuterium exchange and disulfide linkage, Proc. Natl. Acad. Sci. U. S. A. 104 (2007) 7414–7419, http://dx.doi.org/10.1073/pnas.0607745104.
[37] V. Smirnovas, G.S. Baron, D.K. Offerdahl, G.J. Raymond, B. Caughey, W.K. Surewicz, Structural organization of brain-derived mammalian prions examined by hydrogen-deuterium exchange, Nat. Struct. Mol. Biol. 18 (2011) 504–506, http://dx.doi.org/10.1038/nsmb.2035.
[38] W. Swietnicki, M. Morillas, S.G. Chen, P. Gambetti, W.K. Surewicz, Aggregation and fibrillization of the recombinant human prion protein huPrP90-231, Biochemistry 39 (2000) 424–431, http://dx.doi.org/10.1021/bi991967m.
[39] K.W. Leffers, J. Schell, K. Jansen, R. Lucassen, T. Kaimann, L. Nagel-Steger, J. Tatzelt, D. Riesner, The structural transition of the prion protein into its pathogenic conformation is induced by unmasking hydrophobic sites, J. Mol. Biol. 344 (2004) 839–853, http://dx.doi.org/10.1016/j.jmb.2004.09.071.
[40] H. Rezaei, F. Eghiaian, J. Perez, B. Doublet, Y. Choiset, T. Haertle, J. Grosclaude, Sequential generation of two structurally distinct ovine prion protein soluble oligomers displaying different biochemical reactivities, J. Mol. Biol. 347 (2005) 665–679, http://dx.doi.org/10.1016/j.jmb.2005.01.043.
[41] C. Vendrely, H. Valadié, L. Bednarova, L. Cardin, M. Pasdeloup, J. Cappadoro, J. Bednar, M. Rinaudo, M. Jamin, Assembly of the full-length recombinant mouse

prion protein I. Formation of soluble oligomers, Biochim. Biophys. Acta, Gen. Subj. 1724 (2005) 355–366, http://dx.doi.org/10.1016/j.bbagen.2005.05.017.
[42] N. Kachel, W. Kremer, R. Zahn, H.R. Kalbitzer, Observation of intermediate states of the human prion protein by high pressure NMR spectroscopy, BMC Struct. Biol. 6 (2006) 16, http://dx.doi.org/10.1186/1472-6807-6-16.
[43] Y. Zhang, W. Swietnicki, M.G. Zagorski, W.K. Surewicz, F.D. Sonnichsen, Solution structure of the E200K variant of human prion protein. Implications for the mechanism of pathogenesis in familial prion diseases, J. Biol. Chem. 275 (2000) 33,650–33,654, http://dx.doi.org/10.1074/jbc.C000483200.
[44] D.L. Vanik, W.K. Surewicz, Disease-associated F198S mutation increases the propensity of the recombinant prion protein for conformational conversion to scrapie-like form, J. Biol. Chem. 277 (2002) 49,065–49,070, http://dx.doi.org/10.1074/jbc.M207511200.
[45] S. Kiachopoulos, A. Bracher, K.F. Winklhofer, J. Tatzelt, Pathogenic mutations located in the hydrophobic core of the prion protein interfere with folding and attachment of the glycosylphosphatidylinositol anchor, J. Biol. Chem. 280 (2005) 9320–9329, http://dx.doi.org/10.1074/jbc.M412525200.
[46] E.M. Jones, K. Surewicz, W.K. Surewicz, Role of N-terminal familial mutations in prion protein fibrillization and prion amyloid propagation *in vitro*, J. Biol. Chem. 281 (2006) 8190–8196, http://dx.doi.org/10.1074/jbc.M513417200.
[47] M.W. Van Der Kamp, V. Daggett, The consequences of pathogenic mutations to the human prion protein, Protein Eng. Des. Sel. 22 (2009) 461–468, http://dx.doi.org/10.1093/protein/gzp039.
[48] S.H. Bae, G. Legname, A. Serban, S.B. Prusiner, P.E. Wright, H.J. Dyson, Prion proteins with pathogenic and protective mutations show similar structure and dynamics, Biochemistry 48 (2009) 8120–8128, http://dx.doi.org/10.1021/bi900923b.
[49] L.L.P. Hosszu, M.H. Tattum, S. Jones, C.R. Trevitt, M.A. Wells, J.P. Waltho, J. Collinge, G.S. Jackson, A.R. Clarke, The H187R mutation of the human prion protein induces conversion of recombinant prion protein to the prpsc-like form, Biochemistry 49 (2010) 8729–8738, http://dx.doi.org/10.1021/bi100572j.
[50] G. Rossetti, G. Giachin, G. Legname, P. Carloni, Structural facets of disease-linked human prion protein mutants: a molecular dynamic study, Proteins: Struct., Funct., Bioinf. 78 (2010) 3270–3280, http://dx.doi.org/10.1002/prot.22834.
[51] J. Guo, L. Ning, H. Ren, H. Liu, X. Yao, Influence of the pathogenic mutations T188K/R/A on the structural stability and misfolding of human prion protein: insight from molecular dynamics simulations, Biochim. Biophys. Acta, Gen. Subj. 1820 (2012) 116–123, http://dx.doi.org/10.1016/j.bbagen.2011.11.013.
[52] N. Chakroun, S. Prigent, C.A. Dreiss, S. Noinville, C. Chapuis, F. Fraternali, H. Rezaei, The oligomerization properties of prion protein are restricted to the H2H3 domain, FASEB J. 24 (2010) 3222–3231, http://dx.doi.org/10.1096/fj.09–153924.
[53] I. Hafner-Bratkovič, L. Gaedtke, A. Ondracka, P. Veranič, I. Vorberg, R. Jerala, Effect of hydrophobic mutations in the H2-H3 subdomain of prion protein on stability and conversion *in vitro* and *in vivo*, PLoS One 6 (2011), http://dx.doi.org/10.1371/journal.pone.0024238.
[54] J. Singh, J.B. Udgaonkar, The pathogenic mutation T182A converts the prion protein into a molten globule-like conformation whose misfolding to oligomers but not to fibrils is drastically accelerated, Biochemistry 55 (2016) 459–469, http://dx.doi.org/10.1021/acs.biochem.5b01266.
[55] M. Morillas, D.L. Vanik, W.K. Surewicz, On the mechanism of alpha-helix to beta-sheet transition in the recombinant prion protein, Biochemistry 40 (2001) 6982–6987, http://dx.doi.org/10.1021/bi010232q.
[56] A.C. Apetri, W.K. Surewicz, Atypical effect of salts on the thermodynamic stability of human prion protein, J. Biol. Chem. 278 (2003) 22,187–22,192, http://dx.doi.org/10.1074/jbc.M302130200.
[57] R. Riek, S. Hornemann, G. Wider, M. Billeter, R. Glockshuber, K. Wüthrich, NMR structure of the mouse prion protein domain PrP(121-231), Nature 382 (1996) 180–182, http://dx.doi.org/10.1038/382180a0.
[58] A.E. Kelly, H.D. Ou, R. Withers, V. Do, B.B. Corp, T. Hcl, Low-conductivity buffers for high-sensitivity NMR measurements copy is a relatively insensitive method, requiring concentrations, J. Am. Chem. Soc. 124 (2002) 12,013–12,019, http://dx.doi.org/10.1021/ja026121b.
[59] M.W. Voehler, G. Collier, J.K. Young, M.P. Stone, M.W. Germann, Performance of cryogenic probes as a function of ionic strength and sample tube geometry, J. Magn. Reson. 183 (2006) 102–109, http://dx.doi.org/10.1016/j.jmr.2006.08.002.
[60] N. Shimba, H. Kovacs, A.S. Stern, A.M. Nomura, I. Shimada, J.C. Hoch, C.S. Craik, V. Dotsch, Optimization of 13C direct detection NMR methods, J. Biomol. NMR 30 (2004) 175–179, http://dx.doi.org/10.1023/B:JNMR.0000048855.35771.11.
[61] C.J. Roberts, Non-native protein aggregation kinetics, Biotechnol. Bioeng. 98 (2007) 927–938, http://dx.doi.org/10.1002/bit.
[62] R. Murphy, A. Tsai, Misbehaving Proteins Protein (Mis)-Folding, Aggregation, and Stability, Springer-Verlag, New York, 2006.
[63] C.J. Roberts, Kinetics of irreversible protein aggregation: analysis of extended Lumry–Eyring models and Implications for predicting protein shelf life, J. Phys. Chem. B 107 (2003) 1194–1207.
[64] J.M. Andrews, C.J. Roberts, A Lumry–Eyring nucleated polymerization model of protein aggregation kinetics: 1. Aggregation with pre-equilibrated unfolding, 49 (2007) 7897–7913. http://dx.doi.org/10.1021/jp070212j.
[65] P. Debye, E. Huckel, No title, Phys. Z. 24 (1923) 185–206.
[66] R.H. Prion, W. Swietnicki, R. Petersen, P. Gambetti, W.K. Surewicz, pH-dependent stability and conformation of the recombinant human prion protein PrP(90–231), J. Biol. Chem. 272 (1997) 27,517–27,520.
[67] D.O. Alonso, S.J. DeArmond, F.E. Cohen, V. Daggett, Mapping the early steps in the pH-induced conformational conversion of the prion protein, Proc. Natl. Acad. Sci. U. S. A. 98 (2001) 2985–2989, http://dx.doi.org/10.1073/pnas.061555898.
[68] L. Calzolai, R. Zahn, Influence of pH on NMR structure and stability of the human prion protein globular domain, J. Biol. Chem. 278 (2003) 35,592–35,596, http://dx.doi.org/10.1074/jbc.M303005200.
[69] Y. Watanabe, O. Inanami, M. Horiuchi, W. Hiraoka, Y. Shimoyama, F. Inagaki, M. Kuwabara, Identification of pH-sensitive regions in the mouse prion by the cysteine-scanning spin-labeling ESR technique, Biochem. Biophys. Res. Commun. 350 (2006) 549–556, http://dx.doi.org/10.1016/j.bbrc.2006.09.082.

[70] T.C. Bjorndahl, G.P. Zhou, X. Liu, R. Perez-Pineiro, V. Semenchenko, F. Saleem, S. Acharya, A. Bujold, C.A. Sobsey, D.S. Wishart, Detailed biophysical characterization of the acid-induced PrP(c) to PrP(β) conversion process, Biochemistry 50 (2011) 1162–1173, http://dx.doi.org/10.1021/bi101435c.

[71] C.J. Cheng, V. Daggett, Molecular dynamics simulations capture the Misfolding of the bovine prion protein at acidic pH, Biomolecules 4 (2014) 181–201, http://dx.doi.org/10.3390/biom4010181.

[72] S. Hadži, A. Ondračka, R. Jerala, I. Hafner-Bratkovič, Pathological mutations H187R and E196K facilitate subdomain separation and prion protein conversion by destabilization of the native structure, FASEB J. 29 (2015) 882–893, http://dx.doi.org/10.1096/fj.14-255646.

[73] R.P. Honda, K.I. Yamaguchi, K. Kuwata, Acid-induced molten globule state of a prion protein: crucial role of strand 1-helix 1-strand 2 segment, J. Biol. Chem. 289 (2014) 30,355–30,363, http://dx.doi.org/10.1074/jbc.M114.559450.

[74] R.P. Honda, M. Xu, K.I. Yamaguchi, H. Roder, K. Kuwata, A native-like intermediate serves as a branching point between the folding and aggregation pathways of the mouse prion protein, Structure 23 (2015) 1735–1742, http://dx.doi.org/10.1016/j.str.2015.07.001.

[75] L. Miao, H. Qin, P. Koehl, J. Song, Selective and specific ion binding on proteins at physiologically relevant concentrations, FEBS Letters 585 (2011) 3126–3132, http://dx.doi.org/10.1016/j.febslet.2011.08.048.

[76] J.H. Viles, D. Donne, G. Kroon, S.B. Prusiner, F.E. Cohen, H.J. Dyson, P.E. Wright, Local structural plasticity of the prion protein. Analysis of NMR relaxation dynamics, Biochemistry 40 (2001) 2743–2753, http://dx.doi.org/10.1021/bi002898a.

[77] D.B.D. O'Sullivan, C.E. Jones, S.R. Abdelraheim, M.W. Brazier, H. Toms, D.R. Brown, J.H. Viles, Dynamics of a truncated prion protein, PrP(113-231), from15N NMR relaxation: order parameters calculated and slow conformational fluctuations localized to a distinct region, Protein Sci. 18 (2009) 410–423, http://dx.doi.org/10.1002/pro.44.

[78] R.L. Croke, S.M. Patil, J. Quevreaux, D.A. Kendall, A.T. Alexandrescu, NMR determination of pKa values in a-synuclein, Protein Sci. 20 (2011) 256–269, http://dx.doi.org/10.1002/pro.556.

[79] P. Everill, J.L. Sudmeier, W.W. Bachovchin, Direct NMR Observation and pKa determination of the Asp102 side chain in a serine protease, J. Am. Chem. Soc. 134 (4) (2012) 2348–2354.

[80] K. Kuwata, N. Nishida, T. Matsumoto, Y.O. Kamatari, J. Hosokawa-Muto, K. Kodama, H.K. Nakamura, K. Kimura, M. Kawasaki, Y. Takakura, S. Shirabe, J. Takata, Y. Kataoka, S. Katamine, Hot spots in prion protein for pathogenic conversion, Proc. Natl. Acad. Sci. U. S. A. 104 (2007) 11,921–11,926, http://dx.doi.org/10.1073/pnas.0702671104.

[81] E.M. Norstrom, J.A. Mastrianni, The AGAAAAGA palindrome in PrP is required to generate a productive PrP Sc–PrP C complex that leads to prion propagation, J. Biol. Chem. 280 (2005) 27,236–27,243, http://dx.doi.org/10.1074/jbc.M413441200.

[82] S. Jain, J.B. Udgaonkar, Salt-induced modulation of the pathway of amyloid fibril formation by the mouse prion protein, Biochemistry 49 (2010) 7615–7624, http://dx.doi.org/10.1021/bi100745j.

[83] L. Concha-Marambio, R. Diaz-Espinoza, C. Soto, The extent of protease resistance of misfolded prion protein is highly dependent on the salt concentration, J. Biol. Chem. 289 (2014) 3073–3079, http://dx.doi.org/10.1074/jbc.M113.513267.

[84] L.A. Munishkina, J. Henriques, V.N. Uversky, A.L. Fink, Role of protein–water interactions and electrostatics in α-synuclein fibril formation, Biochemistry 43 (11) (2014) 3289–3300.

[85] V. Yeh, J.M. Broering, A. Romanyuk, B. Chen, Y.O. Chernoff, A.S. Bommarius, The Hofmeister effect on amyloid formation using yeast prion protein, Protein Sci. 19 (2010) 47–56, http://dx.doi.org/10.1002/pro.281.

[86] B. Raman, E. Chatani, M. Kihara, T. Ban, M. Sakai, K. Hasegawa, Critical balance of electrostatic and hydrophobic interactions is required for β2-microglobulin amyloid fibril growth and stability, Biochemistry 44 (4) (2005) 1288–1299.

[87] J.S. Pedersen, J.M. Flink, D. Dikov, D.E. Otzen, Sulfates dramatically stabilize a salt-dependent type of glucagon fibrils, Biophys. J. 90 (11) (2006) 4181–4194, http://dx.doi.org/10.1529/biophysj.105.070912.

[88] K. Klement, K. Wieligmann, J. Meinhardt, P. Hortschansky, W. Richter, M. Fändrich, D.- Jena, D.- Jena, D.- Jena, Effect of different salt ions on the propensity of aggregation and on the structure of Alzheimer's A β (1–40) amyloid fibrils, J. Mol. Biol. 373 (5) (2007) 1321–1333, http://dx.doi.org/10.1016/j.jmb.2007.08.068.

[89] F. Chiti, M. Calamai, N. Taddei, M. Stefani, G. Ramponi, C.M. Dobson, Studies of the aggregation of mutant proteins *in vitro* provide insights into the genetics of amyloid diseases, Proc. Natl. Acad. Sci. U. S. A. 99 (2002) 16,419–16,426, http://dx.doi.org/10.1073/pnas.212527999.

[90] M. Calamai, N. Taddei, M. Stefani, G. Ramponi, F. Chiti, S. Biochimiche, V. Uni, V. Morgagni, Relative influence of hydrophobicity and net charge in the aggregation of two homologous proteins, Biochemistry 42 (51) (2003) 15,078–15,083.

[91] J. Juneja, N.S. Bhavesh, J.B. Udgaonkar, R.V. Hosur, NMR identification and characterization of the flexible regions in the 160 kDA molten globule-like aggregate of barstar at low pH, Biochemistry 41 (2002) 9885–9899, http://dx.doi.org/10.1021/bi026034w.

[92] A.J. Baldwin, S.J. Anthony-Cahill, T.P.J. Knowles, G. Lippens, J. Christodoulou, P.D. Barker, C.M. Dobson, Measurement of amyloid fibril length distributions by inclusion of rotational motion in solution NMR diffusion measurements, Angew. Chem. Int. Ed. 47 (2008) 3385–3387, http://dx.doi.org/10.1002/anie.200703915.

[93] A. Sillen, A. Leroy, J.M. Wieruszeski, A. Loyens, J.C. Beauvillain, L. Buée, I. Landrieu, G. Lippens, Regions of tau implicated in the paired helical fragment core as defined by NMR, Chembiochem 6 (2005) 1849–1856, http://dx.doi.org/10.1002/cbic.200400452.

[94] R. Mishra, M. Geyer, R. Winter, NMR spectroscopic investigation of early events in IAPP amyloid fibril formation, Chembiochem 10 (2009) 1769–1772, http://dx.doi.org/10.1002/cbic.200900237.

[95] M.A. Speed, J. King, D.I.C. Wang, Polymerization mechanism of polypeptide chain aggregation, Biotechnol. Bioeng. 54 (1997) 333–343, http://dx.doi.org/10.1002/(SICI)1097-0290(19970520)54:4<333::AID-BIT6>3.0.CO;2-L.

[96] K. Gast, A.J. Modler, H. Damaschun, R. Kro¨ber, G. Lutsch, D. Zirwer, R. Golbik, G. Damaschun, Effect of environmental conditions on aggregation and fibril formation of barstar, Eur. Biophys. J. 32 (2003) 710–723, http://dx.doi.org/10.1007/s00249-003-0336-5.

[97] A.R. Hurshman, J.T. White, E.T. Powers, J.W. Kelly, Transthyretin aggregation under partially denaturing conditions is a downhill polymerization, Biochemistry 43 (2004) 7365–7381, http://dx.doi.org/10.1021/bi049621l.

[98] R. Lumry, H. Eyring, Conformation changes of proteins, J. Phys. Chem. 58 (1954) 110–120, http://dx.doi.org/10.1021/j150512a005.

[99] B.S. Kendrick, J.F. Carpenter, J.L. Cleland, T.W. Randolph, A transient expansion of the native state precedes aggregation of recombinant human interferon-gamma, Proc. Natl. Acad. Sci. U. S. A. 95 (1998) 14,142–14,146, http://dx.doi.org/10.1073/pnas.95.24.14142.

[100] C. Liu, M. Zhao, L. Jiang, P.-N. Cheng, J. Park, M.R. Sawaya, A. Pensalfini, D. Gou, A.J. Berk, C.G. Glabe, J. Nowick, D. Eisenberg, Out-of-register β-sheets suggest a pathway to toxic amyloid aggregates, Proc. Natl. Acad. Sci. U. S. A. 109 (2012) 20,913–20,918, http://dx.doi.org/10.1073/pnas.1218792109.

[101] S.R. Collins, A. Douglass, R.D. Vale, J.S. Weissman, Mechanism of prion propagation: amyloid growth occurs by monomer addition, PLoS Biol. 2 (10) (2004) e321, http://dx.doi.org/10.1371/journal.pbio.0020321.

[102] G. Zettlmeissl, R. Rudolph, R. Jaenicke, Reconstitution of lactic dehydrogenase. Noncovalent aggregation vs. reactivation. 1. Physical properties and kinetics of aggregation, Biochemistry 18 (25) (1979) 5567–5571.

[103] F. Sokolowski, A.J. Modler, R. Masuch, D. Zirwer, M. Baier, G. Lutsch, D.A. Moss, K. Gast, D. Naumann, Formation of critical oligomers is a key event during conformational transition of recombinant Syrian hamster prion protein, J. Biol. Chem. 278 (2003) 40,481–40,492, http://dx.doi.org/10.1074/jbc.M304391200.

[104] K.R. Cho, Y. Huang, S. Yu, S. Yin, M. Plomp, S.R. Qiu, R. Lakshminarayanan, J. Moradian-Oldak, M.S. Sy, J.J. De Yoreo, A multistage pathway for human prion protein aggregation in vitro: from multimeric seeds to beta-oligomers and nonfibrillar structures, J. Am. Chem. Soc. 133 (2011) 8586–8593, http://dx.doi.org/10.1021/ja1117446.

[105] F. Delaglio, S. Grzesiek, G.W. Vuister, G. Zhu, J. Pfeifer, A. Bax, Nmrpipe—a multidimensional spectral processing system based on Unix pipes, J. Biomol. NMR 6 (1995) 277–293.

[106] W. Lee, W.M. Westler, A. Bahrami, H.R. Eghbalnia, J.L. Markley, PINE-SPARKY: graphical interface for evaluating automated probabilistic peak assignments in protein nmr spectroscopy, Bioinformatics 25 (2009) 2085–2087, http://dx.doi.org/10.1093/bioinformatics/btp345.

[107] Y. Shen, F. Delaglio, G. Cornilescu, TALOS+: a hybrid method for predicting protein backbone torsion angles from nmr chemical shifts, J. Biomol. NMR 44 (4) (2009) 213–223, http://dx.doi.org/10.1007/s10858-009-9333-z.